Continued Development of a Fixed-Frequency Albedometer

by

Kathy Dial, B.S.

A Thesis

In

CHEMISTRY

Submitted to the Graduate Faculty
of Texas Tech University in
Partial Fulfillment of
the Requirements for
the Degree of

MASTER OF SCIENCE

Approved

Dr. Jonathan Thompson
Committee Chair

Dr. Dimitri Pappas

Peggy Gordon Miller
Dean of the Graduate School

May, 2011

Copyright 2011, Kathy Dial

Acknowledgements

I am grateful for the help and support my advisor, Dr. Jonathan Thompson, has provided throughout my work at Texas Tech. I have learned much from you, both in the lab and in class. I would also like to thank Dr. Dimitri Pappas for his help and support, as well as agreeing to be on my committee.

Most importantly, I wish to thank my daughter, Elizabeth Dial. You have given me the strength and courage to complete this journey. Finally, I owe a giant thank you to my family and friends, especially my parents, Karon Dial and Joe and Dawn Dial; my sisters, Joy LeFlore and Melissa Arreola; and my brother, Christopher Lay. You have provided me the support and encouragement I needed to complete my degree.

Table of Contents

Acknowledgements ..... **ii**

Abstract ..... **iv**

List of Figures ..... **v**

1. Introduction **1**

1.1 Optical Properties of Aerosols 2
1.2 Measurement of Aerosol Scattering Coefficient (b_{scat}) 4
1.3 Measurement of Aerosol Absorption Coefficient (b_{abs}) 5
1.4 Measurement of Aerosol Extinction Coefficient (b_{ext}) 6
1.7 References 10

2. Simultaneous Measurement of Optical Scattering and Extinction on Dispersed Aerosol Samples **13**

2.1 Introduction 13
2.2 Methods 17
2.3 Results and Discussion 24
2.4 Conclusions 41
2.6 References 52

3. Conclusion **55**

3.1 Major Accomplishments and Findings. 55
3.2 Future directions 56
3.3 References 56

Abstract

Atmospheric aerosols have both direct and indirect effects on climate change. Being able to completely describe the effects will allow scientists to accurately model climate change. This thesis will describe some improvements on the aerosol albedometer, an instrument previously described in the literature. Here, we report on the status of these improvements and the accuracy and precision of the measurements made of the scattering and extinction coefficients (b_{scat} and b_{ext}) with this instrument. We were able to drastically improve the temporal response time, through the use of a glass tube to reduce the sample volume. By comparing optical results to particle concentrations using a condensation particle counter (CPC), we were able to calculate the values of the scattering and extinction cross section (σ_{scat} and σ_{ext}) and compare these to the accepted values calculated from Mie theory. These values agreed within one measurement standard deviation of the accepted values in 13 out of 16 trials. We were also able to observe the increase in relative standard deviations as particle number densities (# particles/cm^3) decreased, giving an idea of how precision scales with concentration of particles. The precision for the measured albedo was shown to be better than that predicted by propagating the uncertainty from b_{scat} and b_{ext} values and associated precisions. Lastly, the effect of light absorbing gases on the measurements was studied in order to understand any potential systematic errors caused by the presence of these gases. It was found that while ozone is of minimal concern, the contribution from NO_2 is of significance and needs to be subtracted out of the measurement.

List of Figures

1.1. The direct and indirect effects of aerosols on radiative forcing.....8

1.2. Setup and data trace for a CRDS instrument. 9

2.1. Illustration of the instrument for simultaneous measurement of scattering and extinction. 43

2.2. The effect of signal averaging time on relative standard deviation.....44

2.3. Instrument response for scattering and extinction coefficient on a polydisperse aerosol sample. 45

2.4. Effect of HEPA filter on the concentration of NO_2 and O_3. 46

2.5. Observed relative precision in scatter coefficient, extinction coefficient, and albedo vs particle number density.....47

2.6. Plot of observed scattering and extinction coefficient vs particle concentration for $(NH_4)_2SO_4$ and nigrosin. 48

2.7. Comparison between measured and theoretical scattering and extinction cross sections (σ_{scat} and σ_{ext}) for $(NH_4)_2SO_4$ and nigrosin aerosol. 49

2.8. Observed average albedo from single point measurements vs particle diameter for $(NH_4)_2SO_4$ aerosol. 50

2.9. Ambient monitoring data from the afternoon of January 22, 2010 during a minor dust episode. 51

Chapter I

Introduction

Understanding atmospheric aerosols is one piece of the puzzle to understanding global climate change. The role they play, however, is anything but simple. Aerosols have both direct and indirect effects on the radiative forcing calculations. This study deals with some of the measurable direct effects, through the interplay between aerosol particles and sunlight. Aerosols directly affect earth's radiative balance through scattering and absorbing light, which changes the amount of light reaching the surface.[1] Indirect effects include increasing cloud condensation nuclei and ice nuclei. The increased number of cloud condensation nuclei decreases the size of the droplets in the cloud, leading to a longer lifetime for the clouds.[2] Increasing ice nuclei has the effect of increasing the precipitation, which shortens the cloud lifetime.[3] With the increased cloud condensation nuclei and ice nuclei, the number of water droplets and ice crystals are increased; both of which increases the amount of light reflected by those clouds.[2, 3] Figure 1.1 depicts both the direct and indirect effects aerosols have on radiative forcing.

Atmospheric aerosols arise from both natural and anthropogenic sources. Some components of aerosols include dust particles, sulfate compounds, and products from biomass burning (this includes both black carbon and organic carbon). Sulfates are scattering, with an albedo of one. Krivacsy and Molnar[4] found the concentration of sulfate particles in Hungary varied from 6.106 $\mu g/m^3$ in the summer to 7.267 $\mu g/m^3$ in the winter, while Meszaros[5] reports the diameter of sulfate particles range in size from 0.125 μm to 1 μm. For biomass burning, the values vary based on the age and source of the

smoke. Dubovik *et al*.[6] report on a study of AERONET data which found the albedo of smoke ranged from about 0.79 up to about 0.985. Guyon *et al*.[7] report on a study of biomass burning in the Amazon tropical forest that found the particle number density to range between about 400 cm^{-3} to about 600 cm^{-3} and the size to range from 0.01 μm to 3.0 μm. The effect of mineral dust again varies, based on the composition and particle size. One study of Saharan dust in Morocco found that the particle sizes ranged from 0.200 μm up to 10 μm, with a median diameter of 0.600 μm.[8] The dominant component of the dust varied with size: for particles up to 0.5 μm, sulfate dominated; above 0.5 μm, the composition was dominated by silicate, quartz, and calcium carbonates. The albedo also varied with composition and size, ranging from 0.89 to 0.96.[8]

1.1 Optical Properties of Aerosols

The direct radiative forcing effect from atmospheric aerosols can be calculated as follows[9]:

$$\Delta F_R = -\left(\frac{1}{4}F_T\right)\left[1-A_C\right]\left(T^2\right)\left[\left(1-R_S\right)^2 2\beta\tau_{scat} - 4R_S\tau_{abs}\right] \qquad (1.1)$$

In this equation, ΔF_R is the radiative forcing (W/m^2), F_T is the average total incoming solar light intensity, T is the fraction of light transmitted through the atmosphere, A_C is the fractional cloud cover, R_S is the surface albedo, β is the upscatter fraction, and τ_{scat} (τ_{abs}) is the optical depth of the aerosol layer due to scattering (absorption). Chylek and Wong[10] list values for each of these variables. Surface albedos are listed as 0.22 over land and 0.06 over ocean. F_T is reported to be 1370 W/m^2, T is reported as 0.79, and A_C is reported as 0.6. The remaining values are reported for smoke aerosol. For small, fresh

biomass burning aerosols, β is 0.37; for large, aged aerosols, β is 0.11. Finally, τ_{abs} is 0.0026 and τ_{scat} is 0.030. The optical properties of aerosols measured in this study contribute to τ_{scat} and τ_{abs}.

The Beer-Lambert Law models the attenuation of light by aerosols,

$$I = I_o \times e^{-(b_{ext} \cdot Z)} \tag{1.2}$$

In this equation, I and I_0 are the intensity of light at the detector and source, respectively; b_{ext} is the extinction coefficient of the aerosol (m^{-1}); and Z is the pathlength (m). Since aerosols attenuate light by both scattering and absorption, b_{ext} can be expressed as the sum of the scattering and absorption coefficients (b_{scat} and b_{abs}),

$$b_{ext} = b_{abs} + b_{scat} \tag{1.3}$$

The scattering cross section is related to the scattering coefficient (b_{scat}), as follows:

$$b_{scat} = \sigma_{scat} \times N \tag{1.4}$$

Here, N is the particle density (m^{-3}). The absorption cross section (σ_{abs}) and extinction cross section (σ_{ext}) are related to b_{abs} and b_{ext} in the same way.

The absortion and scattering cross sections are related to the optical depth terms from Eq. 1.1 as follows:

$$\tau_{scat} = \sigma_{scat} \times N \times Z \tag{1.5}$$

Since σ_{scat} (σ_{abs}) has units of m^2 and Z has units of m, τ_{scat} (τ_{abs}) is dimensionless.

Another useful parameter is the single-scattering albedo (ω), which is the ratio of the amount of light scattered by a particle to the amount of light both scattered and absorbed. It can be calculated using the extinction and scattering coefficients:

$$\omega = \frac{b_{scat}}{b_{ext}} \tag{1.6}$$

This ratio can have a large effect on the direct effect of aerosols; Penner[11] notes that a change as small as 0.9 to 0.8 can reverse the sign of the calculated radiative forcing.

1.2 Measurement of Aerosol Scattering Coefficient (b_{scat})

The scattering coefficient is often measured using nephelometry. The integrating nephelometer is designed to integrate the scattering signal over all angles.[12, 13] A common design of the instrument consists of a long tube into which the sample is introduced and illuminated. The detector is placed at one end and the source is at the middle.[14] This allows particles in all portions of the instrument to scatter light, at all different angles. Because it is not actually physically possible to measure the extreme forward or backward scatter, integrating nephelometers underestimate b_{scat} through the truncation error. Truncation angles are typically in the range of 5° to 15°, and can change depending on particle size and how spherical the particle is.[15, 16] Another type of nephelometer is the integrating sphere nephelometer. Here the sample chamber is a sphere, with a detector on the side of the sphere.[17] The sphere allows for the measurement of extreme back and forward scatter. Varma *et al*.[17] described an integrating sphere nephelometer that includes truncation reducing tubes that the laser beam travels through on entering and exiting the sphere. This lowers the truncation angle

to around 1°, resulting in a more accurate measurement of b_{scat}. The albedometer described later in this work was heavily influenced by this seminal work.

1.3 Measurement of Aerosol Absorption Coefficient (b_{abs})

There are several instruments in current use for measuring the absorption coefficient. These methods can be classified as filter based measurements or measurements on dispersed samples.

1.3.1 Filter based measurements

Filter based measurements consist of depositing aerosol particles onto a filter, then measuring the transmittance of light through the sample spot and a reference to get b_{abs}. The reference can either be a second, blank filter or a blank spot on the same filter. Two common instruments are the aethalometer and the particle soot absorption photometer (PSAP).[18-21] Both methods are attractive because they are simple to use, relatively inexpensive, and absorption by gases does not affect the measurement.[22] However, if a correction is not employed, scattering particles can lead to an overestimation of b_{abs}.[19,21] Filter effects, such as loading effects,[18,19] can also be a problem.

1.3.2 Measurements on dispersed samples

Two methods for measuring b_{abs} on dispersed samples are photoacoustic spectroscopy and photothermal interferometry. Both methods are based on the concept that particles absorbing light will experience a temperature increase, which is then transferred to the surrounding air. For photoacoustic spectroscopy, this creates a pressure differential, which can be detected as sound waves.[23,24] While this method has been

shown to be sensitive, semi-volatile compounds do interfere with the measurement. This occurs when the heat is dissipated through evaporation of the semi-volatile, rather than through transfer to the surrounding air.[20] In photothermal interferometry, the dissipation of heat to the surrounding air is detected through the change in refractive index of the air.[25, 26] This method experiences the same interferences from semi-volatile compounds, with one added complication: the vapors from the semi-volatile will further change the refractive index, due to the mixing of air with another component.[20]

1.4 Measurement of Aerosol Extinction Coefficient (b_{ext})

While the extinction coefficient of aerosols is often calculated from b_{abs} and b_{scat}, it can also be measured. Cavity ringdown spectroscopy (CRDS) has been used to measure b_{ext}.[27- 35] CRDS grew out of a need to characterize highly reflective mirror surfaces.[36] In CRDS, a cavity is formed with two (or more) highly reflective mirrors. A laser is shot through one mirror and a detector is placed behind the other. The light bounces between the mirrors, but a small amount goes through with each pass and the intensity of the light undergoes an exponential decay. Figure 1.2 shows a typical setup for a CRDS instrument along with a data trace.

The ringdown time constant, τ, is the time it takes for the intensity to reach e^{-1} of the initial pulse.[37] The sensitivity of the techniques comes from the fact that the light will often traverse the cavity thousands of times, resulting in a very long effective pathlength. The limit of detection for CRDS systems for b_{ext} has been reported from as low as 0.20 Mm^{-1} to 1 Mm^{-1}. [28, 34, 35]

When a sample is present in the cavity, τ will decrease due to the added loss of light through scattering and/or absorption. For a sample, τ can be related to b_{ext} as follows:

$$b_{ext} = \frac{1}{c}\left(\frac{1}{\tau_{sample}} - \frac{1}{\tau_{cavity}}\right) \tag{1.7}$$

where τ_{sample} and τ_{sample} are the ringdown time constants for the sample and the empty cavity, repectively and c is the speed of light in a vacuum.

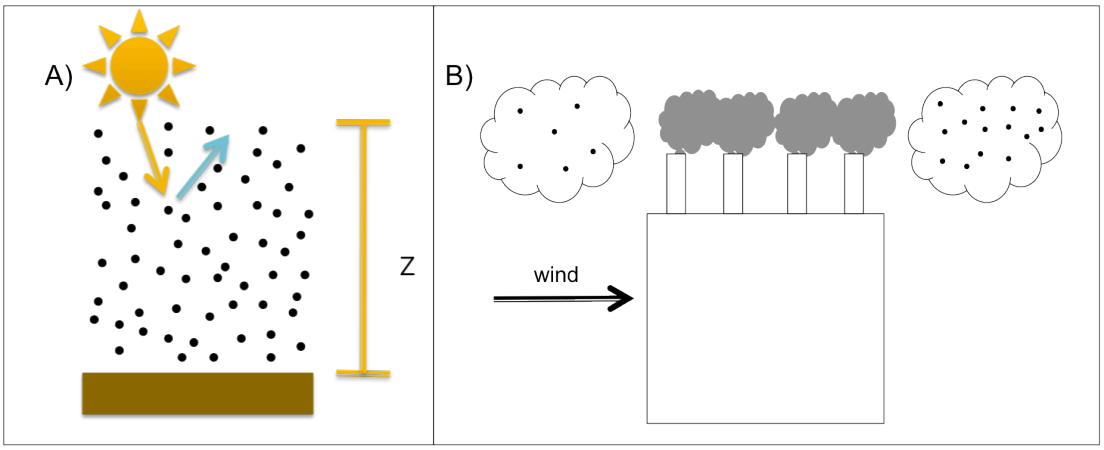

Figure 1.1. The direct and indirect effects of aerosols on radiative forcing.
A) Direct effects result from absorption and scattering of solar radiation. Absorption results in a warming effect, while scattering results in a cooling effect. B) Increase in cloud condensation nuclei from aerosol particles increases both the reflectivity of the cloud as well as the cloud lifetime.

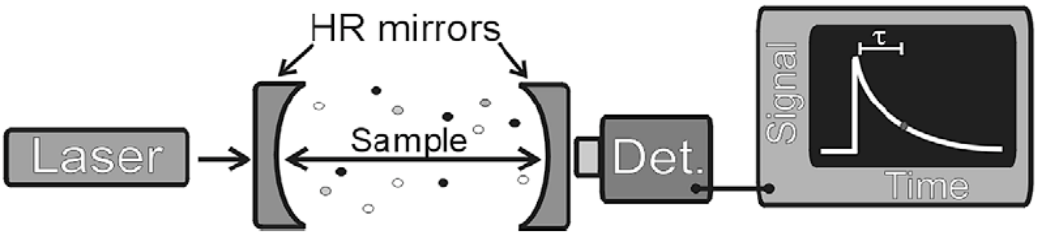

Figure 1.2. Setup and data trace for a CRDS instrument. Two highly reflective mirrors form a sample cavity, and light is bounced between them. With each pass, a small amount leaks through the mirrors. τ is measured for the empty cavity and with a sample present, then Eq. 1.7 is used to calculate b_{ext}.

1.7 References

[1] Ramaswamy, V. In *Climate Change 2001: The Scientific Basis. Contribution of Working Group I to the Third Assessment Report of the Intergovernmental Panel on Climate Change*; Houghton, J. T., Ed.; Cambridge University Press: Cambridge, U.K., **2001**, p 349.

[2] Boucher, O.; Lohmann, U. *Tellus B* **1995**, *47*, 281.

[3] Lohmann, U.; Feichter, J. *Atmospheric Chemistry and Physics* **2005**, *5*, 715.

[4] Krivacsy, Z.; Molnar, A. *Atmospheric Research* **1998**, *46*, 279.

[5] Meszaros, E.; Barcza, T.; Gelencser, A.; Hlavay, J.; Kiss, G.; Krivacsy, Z.; Molnar, A.; Polyak, K. *Journal of Aerosol Science* **1997**, *28*, 1163.

[6] Dubovik, O.; Holben, B.; Eck, T. F.; Smirnov, A.; Kaufman, Y. J.; King, M. D.; TanrÈ, D.; Slutsker, I. *Journal of the Atmospheric Sciences* **2002**, *59*, 590.

[7] Guyon, P.; Graham, B.; Beck, J.; Boucher, O.; Gerasopoulos, E.; Mayol-Bracero, O. L.; Roberts, G. C.; Artaxo, P.; Andreae, M. O. *Atmospheric Chemistry and Physics* **2003**, *3*, 951.

[8] Schladitz, A.; M¸ller, T.; Kaaden, N.; Massling, A.; Kandler, K.; Ebert, M.; Weinbruch, S.; Deutscher, C.; Wiedensohler, A. *Tellus B* **2009**, *61*, 64.

[9] Finlayson-Pitts, B. J.; Pitts, J. N.; Corporation, E. *Chemistry of the upper and lower atmosphere: Theory, experiments, and applications*; Academic press San Diego, **2000**; Vol. 1040.

[10] Chylek, P.; Wong, J. *Geophysical Research Letters* **1995**, *22*, 929.

[11] Penner, J. E. In *Climate Change 2001: The Scientific Basis. Contribution of Working Group I to the Third Assessment Report of the Intergovernmental Panel on Climate Change*; Houghton, J. T., Ed.; Cambridge University Press: Cambridge, U.K., **2001**, p 289.

[12] Ruby, M. G.; Waggoner, A. P. *Environmental Science & Technology* **1981**, *15*, 109.

[13] Heintzenberg, J.; Charlson, R. J. *Journal of Atmospheric and Oceanic Technology* **1996**, *13*, 987.

[14] Radiance Research *Operation Procedures M903 Nephelometer* Seattle, WA.

[15] Moosmuller, H.; Arnott, W. P. *Review of Scientific Instruments* **2003**, *74*, 3492.

[16] Muller, T.; Nowak, A.; Wiedensohler, A.; Sheridan, P.; Laborde, M.; Covert, D. S.; Marinoni, A.; Imre, K.; Henzing, B.; Roger, J. C. *Aerosol Science and Technology* **2009**, *43*, 581.

[17] Varma, R.; Moosmuller, H.; Arnott, W. P. *Optics Letters* **2003**, *28*, 1007.

[18] Arnott, W. P.; Hamasha, K.; Moosmuller, H.; Sheridan, P. J.; Ogren, J. A. *Aerosol Science and Technology* **2005**, *39*, 17.

[19] Bond, T. C.; Anderson, T. L.; Campbell, D. *Aerosol Science and Technology* **1999**, *30*, 582.

[20] Moosmuller, H.; Chakrabarty, R.; Arnott, W. *Journal of Quantitative Spectroscopy and Radiative Transfer* **2009**, *110*, 844.

[21] Sheridan, P.; Arnott, W.; Ogren, J.; Andrews, E.; Atkinson, D.; Covert, D.; Moosmuller, H.; Petzold, A.; Schmid, B.; Strawa, A.; Varma, R.; Virkkula, A. *Aerosol Science & Technology* **2005**, *39*, 1.

[22] Moosmuller, H.; Chakrabarty, R. K.; Arnott, W. P. *Journal of Quantitative Spectroscopy & Radiative Transfer* **2009**, *110*, 844.

[23] Arnott, W. P.; Moosmuller, H.; Rogers, C. F.; Jin, T.; Bruch, R. *Atmospheric Environment* **1999**, *33*, 2845.

[24] Lack, D. A.; Lovejoy, E. R.; Baynard, T.; Pettersson, A.; Ravishankara, A. R. *Aerosol Science and Technology* **2006**, *40*, 697.

[25] Sedlacek III, A. J. *Review of Scientific Instruments* **2006**, *77*, 064903.

[26] Sedlacek, A.; Lee, J. *Aerosol Science and Technology* **2007**, *41*, 1089.

[27] Atkinson, D. B. *Analyst* **2003**, *128*, 117.

[28] Baynard, T.; Lovejoy, E. R.; Pettersson, A.; Brown, S. S.; Lack, D.; Osthoff, H.; Massoli, P.; Ciciora, S.; Dube, W. P.; Ravishankara, A. R. *Aerosol Science and Technology* **2007**, *41*, 447.

[29] Bulatov, V.; Fisher, M.; Schechter, I. *Analytica Chimica Acta* **2002**, *466*, 1.

[30] Miles, R. E. H.; Rudic, S.; Orr-Ewing, A. J.; Reid, J. P. *Physical Chemistry Chemical Physics* **2010**, *12*, 3914.

[31] Moosmuller, H.; Varma, R.; Arnott, W. P. *Aerosol Science and Technology* **2005**, *39*, 30.

[32] Richman, B. A.; Kachanov, A. A.; Paldus, B. A.; Strawa, A. W. *Optics Express* **2005**, *13*, 3376.

[33] Smith, J. D.; Atkinson, D. B. *Analyst* **2001**, *126*, 1216.

[34] Thompson, J. E.; Smith, B. W.; Winefordner, J. D. *Analytical Chemistry* **2002**, *74*, 1962.

[35] Thompson, J. E.; Nasajpour, H. D.; Smith, B. W.; Winefordner, J. D. *Aerosol Science and Technology* **2003**, *37*, 221.

[36] O'Keefe, A.; Scherer, J.; Paul, J.; Saykally, R. In *Cavity-ringdown spectroscopy: an ultratrace-absorption measurement technique*; Busch, K. W., Busch, M. A., Eds.; ACS Publications: **1999**; Vol. 720, p 71.

[37] Busch, K. W.; Busch, M. A. In *Cavity-ringdown spectroscopy: an ultratrace-absorption measurement technique*; Busch, K. W., Busch, M. A., Eds.; ACS Publications: **1999**; Vol. 720, p 7.

Chapter II

Simultaneous Measurement of Optical Scattering and Extinction on Dispersed Aerosol Samples

2.1 Introduction

Developing a more precise understanding of earth's climate system vis-à-vis climate variability and change has important consequences for sustainable and strategic development. The latest Intergovernmental Panel on Climate Change (I.P.C.C.) report estimates a radiative forcing of +2.63 ± 0.26 W/m^2 for well-mixed greenhouse gases, suggesting a significant warming influence.[1] Atmospheric particulate matter (aerosols) can also directly influence climate by scattering or absorbing sunlight in the atmosphere (heating atmosphere aloft, reducing surface irradiance). Aerosols can also alter the spatial and temporal distribution and/or optical properties of clouds, which can indirectly influence surface temperatures and precipitation patterns.[2 - 4]

At present, the effects of atmospheric particulate matter remain the least precisely known variable in earth's climate system. The latest I.P.C.C. radiative forcing estimate for the direct aerosol effect is -0.50 W/m^2; however, the relative uncertainty associated with this estimate is 80% of the value. The indirect aerosol effect is even less precisely known. The current 95% confidence range is -0.30 to 1.8 W/m^2. The negative radiative forcing values indicate a cooling tendency, so aerosols may offset the greenhouse gas forcing to a significant extent. However, when propagating uncertainty in net radiative forcing, the uncertainty in the result is dominated by the least precisely known value. As such, constraining uncertainty on estimates of the aerosol's direct and indirect effect is of substantial societal importance.

Early estimates of anthropogenic aerosol climate forcing treated aerosols only as scatterers.[5] Subsequently, the role of light absorbing aerosol components such as soot, mineral dusts, or the nebulous class of material referred to as brown-carbon have been considered.[6-11] The extent of each optical effect can be quantified through the absorption (b_{abs}) and scattering (b_{scat}) coefficients of the aerosol cloud. The extinction coefficient (b_{ext}) of an aerosol cloud is the sum of scattering (b_{scat}) and absorption coefficients (b_{abs}). The aerosol single scatter albedo (SSA) is the ratio of scattering to extinction coefficients. Equations 1 and 2 summarize and define these relationships.

$$b_{ext} = b_{abs} + b_{scat} \tag{1}$$

$$\omega = \frac{b_{scat}}{b_{ext}} \tag{2}$$

The direct radiative forcing of an aerosol layer is a complicated interplay between light scattering and absorption. Scattering leads to cooling effect, while absorbing aerosols warm the atmosphere aloft. Therefore, estimation of direct aerosol forcing requires knowledge of aerosol scattering and extinction coefficients and their ratio (albedo) to a high degree of accuracy and precision.

Equations 1 and 2 suggest single scatter albedo (SSA) can be computed through simultaneous measurements of aerosol scattering and either extinction or absorption. Measurement of aerosol extinction is complicated by the relatively low optical losses encountered ($b_{ext} < 100$ Mm^{-1} is typical) so highly sensitive techniques are required. To meet these demands, cavityenhanced spectroscopy has become a popular choice for direct measurement of aerosol extinction.[12-29] The scattering coefficient is often determined

through conventional integrating nephelometry.[30] A drawback to traditional nephelometers is light scattered very near the forward and reverse direction (often with 5-15° of forward and reverse) cannot be measured accurately leading to an underestimation of the scattering coefficient.[31-34] This is known as truncation error. Fortunately, correction schemes for several commercially available nephelometers have been developed to help account for this limitation.[35, 36] More recently, use of reciprocal nephelometers such as the integrating sphere nephelometer have also been employed to address this shortcoming.[37, 38] These devices decrease the truncation angle to roughly 1° in certain designs. Several investigators have simultaneously made considerable progress in the direct measurement of the aerosol absorption coefficient (b_{abs}) through the use of photoacoustic spectroscopy and photothermal interferometry.[39-47]

Recently, our group has reported on a first generation instrument to simultaneously measure scattering and extinction on a dispersed aerosol sample.[48] This technique performs cavity ringdown spectroscopy (CRDS) on an aerosol sample within an integrating sphere nephelometer. Light scattered from the probe laser beam is collected by the sphere and monitored through a separate detection channel. The ring-down experiment provides an aerosol extinction coefficient (b_{ext}), and the scatter coefficient (b_{scat}) is monitored on the separate channel through calibration with a gas of known optical properties. We believe this platform offers several potential measurement advantages. Simultaneous measurement of scatter and extinction within the exact same probe volume could reduce the measurement uncertainty due to two instruments being presented with slightly different samples and/or reduce fluctuations in data caused by

statistical variability in the number of particles within the probe beam (vide infra). Measurements on dispersed aerosols also eliminate potential artifacts associated with filter sampling[49, 50] and potentially allow study of the effect of relative humidity on aerosol albedo. The initial demonstration of this technology did have several caveats. A major disadvantage was the temporal response of the instrument. The sphere itself was 50 L in volume and required approximately 30 min to fill/flush. This would be unacceptable for certain monitoring applications such as on-board aircraft. Additionally, the aerosol sample was introduced into the sphere at an arbitrary location on its surface. This did not constrain the optical path length as well as desired. Furthermore, automated calibration and monitoring protocols were not established, measurement accuracy was not validated through Mie theory, and measurement precision was not optimized or closely examined.

In this work, we describe and characterize a second-generation instrument for simultaneous measurement of aerosol scattering and extinction on a dispersed aerosol. Efforts have been made to characterize and optimize the precision with which the optical measurements can be made. The effects of instrument noise, gas-phase absorbers, and statistical fluctuations in the number of particles within the probe beam are considered. The level of precision achieved is compared with measurements previously reported in the literature for alternative measurement techniques. Additionally, both scattering and extinction measurements are validated through Mie theory for size-selected aerosols of known composition. Aerosol optical data collected on a dust-dominated aerosol at our location is also presented.

2.2 Methods

The general measurement approach described in our previous work[48] has been conserved. There have been several changes in implementing the approach that will be summarized here. Figure 1 illustrates the second-generation instrument for measurement of scattering and extinction by aerosols.

2.2.1 Description of the Measurement Cell and Sample Inlet

The device consists of two 30.5 cm diameter stainless steel hemispheres that are welded to square 35.5 cm flanges and bolted together. All inner surfaces of the sphere were coated with Duraflect, a proprietary diffuse reflectance coating applied by Labsphere, Inc. that exhibits a reflectance >95% between λ = 350 and 1200 nm. A 2.54 cm wide light baffle fabricated from stainless steel was placed in an arc within the interior of the sphere. The baffle was also coated with Duraflect coating. The baffle's position was strategically chosen to block the laser beam from being scattered directly into the scattering detector's field of view. This assures all light collected by the scattering detector must have undergone at minimum 1 reflection off the sphere's surface prior to being detected.

Perhaps the most significant change from the previous design is the use of a 3.8 cm diameter transparent tube (Pyrex 7740) to contain the aerosol sample within the integrating sphere. The 38.1 cm long tube was fabricated from commercially available vacuum components (460013, MDC Vacuum) and a short length of 3.8 cm diameter tubing. This tube reduces sample volume to only ≈0.4 L (previously 50 L), which drastically reduces instrument time response when compared to the previous version. The

tube also better constrains the optical path. Each tube is terminated by a standard 2.75 in. CF flange, and the first few centimeters of each tube is stainless steel before the metal to glass seal. The metallic inner surfaces of these tubes were also coated with Duraflect. These flanges were mated to a 2.54 cm thick double sided 2.75 in. CF flange (140014, MDC Vacuum) with a standard copper gasket. A 1.27 cm hole was drilled through the side of this flange to fit a 15 cm length of 1.27 cm diameter stainless steel tubing. These tubes were silver soldered in place and serve as the means to introduce/remove sample from the measurement chamber. The opposite side of the double sided flange was mated to a 2.75 in. CF flange that was part of the commercially available mirror mounts (Los Gatos Research). These flanges were mated with a special gasket fabricated from copper and coated on one side with Duraflect. A 0.635 cm diameter hole was drilled in the center of this gasket to allow for the probe beam to pass. The mirror mounts themselves were equipped with 1/8 in. diameter stainless tubes that were used for mirror purge lines and for filling the optical cell with calibration gases when desired. Gases in the mirror purge lines were filtered with an in-line Wafergard filter and metered with a combination of a needle valve/rotameter. Typical mirror purge flow rates were <500 mL/min. The calibration gas (1,1,1,2-tetrafluoroethane (R- 134a)) was also added to the measurement cell via the mirror purge lines. Addition of the calibration gas was controlled by the instrument control software and a second solenoid valve (Asco).

The inlet tubing to the optical cell was plumbed into a short length of 1/2 in. diameter conductive silicone tubing that ran to a 1/2 in. stainless steel mixing tee. One port of the tee (straight shot) was connected to a ball valve (Duravalve DR2A) through a

short length of 1/2 in. stainless steel tubing. The other port was routed through a HEPA particle filter (Pall 12144) and a solenoid valve (Asco). Both valves were controlled by the data acquisition software. A second mixing tee was used to combine the flow channel again. Independent control of both valves allows switching between aerosol samples and filtered air blanks.

At the optical cell exit, sensors for pressure (MKS Instruments 722A13TCD2FA) and relative humidity/temperature (Vaisala, HMP50) were placed within a cylindrical tube. These sensors were monitored by the instrument control software to account for changes in cell pressure and temperature that occurred since the last calibration was performed. Typical pressure inside the sphere was ~690-700 mmHg, and temperatures ranged between 20 and 25 °C. The tube outlet was then routed to either a condensation particle counter (CPC) or mass flow controller (MFC)/air pump depending on the experiment. Experiments using the CPC involved a sample flow rate through the cell of 1 L/min or less. Sample flow rates on the order of 8 L/min were employed when the MFC and air pump were employed. The air pump was also turned on/off under computer control.

2.2.2 Optical Measurements

Briefly, aerosol extinction is monitored by cavity ring-down spectroscopy. This technique measures the time constant (τ) of an optical resonator following a laser pulse. The time constant can be related to extinction coefficient of the sample placed between the high reflectivity mirrors by

$$\tau = \frac{t_r}{2[(1-R)+b_{ext}L]} \tag{3}$$

where t_r is the round trip transit time for the beam, R is the mirror reflectivity, L is the cavity length, and b_{ext} is the sample's extinction coefficient. In a typical experiment, L and R are held constant and the aerosol extinction coefficient can be extracted from knowledge of the ring-down time constants observed for the sample (τ_{sam}) and when filtered air (τ_{air}) fills the measurement cell through the following equation:

$$b_{ext} = \frac{1}{c}\left(\frac{1}{\tau_{sam}} - \frac{1}{\tau_{air}}\right) \tag{4}$$

The values of b_{ext} computed through these equations are spatially averaged over the entire optical cell. When aerosol measurements are made via CRDS, it is common to purge the mirror housings with clean air to prevent particle deposition. In order to correct for this we multiply the result obtained through eq 4 by the ratio of the distance between the mirrors and the optical path the particles actually occupy (ratio for our cell = 1.06). This is an acceptable practice so long as the extinction of air is considered "zero". By taking our spectroscopic blank on filtered air, we aim to effectively subtract out the contribution of air to extinction. The chemical composition of this blank sample is of significant consequence, however, since light absorbing gases (NO_2 or O_3 for our λ) present in the sample can interfere with aerosol measurements. This will be discussed in more detail later. All b_{ext} values reported in this article refer only to the aerosol contribution, that is, they have been air subtracted.

We have employed a frequency doubled (λ = 532 nm) Nd: YAG laser (Quantel, Brio) pulsed at 20 Hz. This laser is rated by the manufacturer for maximum pulse energies of 60-70 mJ contained within 3-5 ns pulses; however, in practice we operate at much lower energies. The beam is approximately 4 mm in diameter, is vertically polarized, and has a divergence of <0.6 mrad. The CRDS cell employs a symmetrical optical resonator formed from two 6 m radius of curvature, 2.54 cm diameter high reflectivity mirrors (R > 0.9999). The mirrors were placed 44.5 cm apart. The CRDS signal was monitored by a standard photomultiplier tube (931B, Hammamatsu) mounted in a light-tight metallic shield fastened to the output mirror housing. In order to avoid saturation of the photomultiplier, the CRDS output beam was attenuated by a neutral density filter prior to measurement. Light scattered by the aerosol sample was collected by the inner surface of the integrating sphere, and a fraction of this light was directed to a separate photomultiplier tube (H7732P-1, Hammamatsu) that was affixed to the surface of the sphere.

Signal from both PMTs were sampled using a 14 bit, 200 Msample/s digitizer card (Gage Applied, Compuscope 14200). Acquisition of data was triggered by the Q-switch sync line of the Nd:YAG laser. Software written in LabView (National Instruments) was used to acquire and process data from the fast DAQ card and to collect temperature, relative humidity, and pressure data through a separate USB data acquisition device (National Instruments, NI USB-6008). After acquisition of the RD transient, the signal was normalized to a 0-1 scale and the natural logarithm of the signal computed. The natural log of the signal in time was then plotted and a line was fit to the data. The

slope of this line was extracted and used to compute the ring-down time constant. This scheme was adapted for the second version of the instrument since it is computationally much faster than the nonlinear curve fitting procedure employed in the first generation instrument. The nonlinear fitting scheme was the rate-limiting step in terms of collecting data in the first generation instrument. In addition, the software is programmed to divide the scatter channel signal by the original (not normalized) CRDS channel signal (I_{scat}/I_{CRDS}) at every point along the ring-down transient. The software then extracts 2000 individual values and averages them to report an I_{scat}/I_{CRDS} ratio. In our previous work and that of Strawa *et al.*,[21] this ratio has been shown to scale linearly with scattering coefficient (b_{scat}). This ratio is measured and correlated to the scatter coefficient through calibration with R-134a gas as described in our previous work.

In practice, the instrument is automatically calibrated under computer control. The calibration routine begins by closing both the sample ball valve and R-134a valves and opening the filtered air bypass valve. The air pump is then turned on and allowed to run for 150 s, after which the data is collected for the filtered air. Next the air pump is turned off and the bypass valve is closed, while the R-134a and aerosol sample ball valves are opened. The cell is allowed to fill for 200 s, and then data collection occurs. The final stage of calibration is closing the R-134a valve and turning on the air pump to flush the cell with sample for 40 s.

2.2.3 Additional Methods

A TSI electrostatic classifier (3080) was used with a 3081 long differential mobility analyzer (DMA) to size select aerosol particles for analysis. Aerosol sample

flow was always adjusted to <10· the sheath flow to maintain a narrow particle size distribution. This was accomplished through a makeup flow valve and HEPA filter installed at the inlet to the CPC. Measured particle concentrations were corrected for this dilution. Our data is not corrected for scattering/extinction by multiply charged particles since we chose particle sizes that were large enough that particles of larger size would either not be present or removed by inertial impaction at the inlet to the classifier and therefore not measured. It should be noted that initial experiments using smaller diameter particles (d_p < 400 nm) often yielded erroneous optical cross sections without correction. A TSI 3772 butanol based CPC was used to measure particle number density (no. of particles/cubic centimeter) during experiments. The Mieplot software written by Phillip Lavin was employed to compute Mie efficiency parameters (Q_{scat}, Q_{ext}, Q_{abs}). For these calculations, we have used the refractive indices of ammonium sulfate (m = 1.52 + 0.00i) and nigrosin dye (m = 1.72 + 0.28i) that have been reported by Lang-Yona *et al*.[22] The aerosol particles are generated using a TSI model 9302 atomizer operated at roughly 1030 mmHg gauge pressure. In order to lower the relative humidity of the particles, the stream is passed through a heated tube and into a large mixing chamber. The particles then pass through a TSI model 3062 diffusion dryer, followed by a second, homemade, diffusion dryer. The now dry particles pass through PVC pipe and 3/8 in. tubing to a flask that is connected to the sample inlet tubing for the setup.

2.3 Results and Discussion

2.3.1 Effect of Signal Averaging Time on Precision

In an effort to optimize collection of data, we have examined the effect of signal averaging time on measurement precision. This study was carried out on a sealed cell containing filtered air to ensure measurements represent fundamental instrumental limits on precision. Figure 2 illustrates the observed relative standard deviation of the scatter ratio (I_{scat}/I_{CRDS}) and ring-down time (τ) as a function of signal averaging time for this experiment. The solid line on each plot represents a $1/\sqrt{t}$ (effectively $1/\sqrt{N}$) scaling pattern that would be expected from measurement theory. As observed, measurement precision improves in general agreement with $1/\sqrt{t}$. Additionally, only minor improvements in precision were achieved beyond approximately 3 s integration time. This suggests adequate measurement precision can be achieved in only a few seconds for applications requiring rapid time response (such as on-board aircraft).

2.3.2 Instrument Temporal Response

A major difference in the apparatus described herein, and the previous method[48] is the inclusion of a transparent tube to contain the aerosol sample. The tube reduces the sample cell volume to approximately 0.4 L (from ≈50 L). In addition, use of the tube better defines the sample flow path through the instrument. Previously, aerosol was added directly to the sphere at an arbitrary location on its surface. In this instrument, the sample is added through the 2.75 in. CF flange. Likewise, the aerosol exits through a second CF flange at the opposite end of the tube. This constrains the effective sample path length. Use of commercially available vacuum components is also convenient and assures airtight seals. The latter is of consequence for potential operations on board aircraft.

Given the drastic change in tube volume, re-evaluation of the instrument time response was considered.

To determine the temporal response of the method, an experiment was run in which b_{ext} and b_{scat} were monitored through time. Figure 3 shows the results. Initially, filtered air flushed the chamber for approximately 20 min. Then, ammonium sulfate particles (polydisperse, submicrometer) were added to the sphere, and within one update of the software, both b_{ext} and b_{scat} had gone up to ≈130 Mm^{-1}. Data was collected on the particles for approximately 30 min, and the particle generation system was turned off. Again, both b_{ext} and b_{scat} returned to zero within one to two updates. It is believed the slight drift down in measured b_{scat} and b_{ext} is a consequence of the particle generation system. The time required for one software update was approximately 58 s. At present, the temporal response is limited by the signal averaging protocol used in the instrument control software. Again, the previous version of the integrating sphere had an internal volume of 50 L. This large volume afforded a time response of 20-30 min at typical sampling flow rates (≈ 8 L/min). Use of the transparent tube allows reduction in total sample volume to <1% of the original version and a reduction in temporal response to <1 min. It is envisioned that if fewer signal averages are employed, this time response may be decreased further.

2.3.3 Effect of Light Absorbing Gases on Extinction Measurement

While any light absorbing gas could potentially lead to measured extinction (and, therefore, interference with aerosol measurements), only ozone and NO_2 are generally thought to be of significance for the midvisible spectral region. Ozone contributes an

optical loss of ≈0.00605 Mm^{-1} per ppb O_3 under our measurement conditions while the stronger absorber NO_2 contributes ≈0.33 Mm^{-1} per ppb at 532 nm. Typical tropospheric ozone mixing ratios are 30-40 ppb leading to extinction <<1 Mm^{-1} for 532 nm. The concentration of NO_2 is more variable depending on distance from source, however mixing ratios exceeding 200 ppbv have been reported for urban areas. Clearly, optical extinction by these gases should be considered and deconvoluted from aerosol extinction. This common problem is nearly universally addressed by performing periodic filtered air blank measurements. In this approach, particles are removed from the air stream by a highly efficient filter and optical measurements made. Presumably, the absorbing gas is unaffected by the particle filter and passes into the optical cell. Setting this sample as the spectroscopic blank removes the influence of the absorbing gas on subsequent measurements of aerosol extinction with nonfiltered airstreams. However, if passing the sample through the filter line alters the concentration of absorbing gases differently when compared to the unfiltered sample inlet, the possibility for systematic error arises. The HEPA filters we use here (Pall 12144) feature a polypropylene housing with a membrane formed from an acrylic copolymer. It is therefore possible that filtration could alter concentrations of reactive gases such as ozone. The paragraph that follows examines the significance of this potential problem.

Figure 4 illustrates an experiment in which air containing an elevated concentration of (A) NO_2 and (B) ozone was added to our measurement cell through the sampling line at 8.3 L/min. For the experiment shown in part A, two experimental trials were performed in which the gas-stream containing an elevated level of NO_2 was

sequentially routed through the aerosol inlet and then diverted through a particle filter line (HEPA filter). From 0 to 10 min and 30 to 45 min, the gas stream was routed through the aerosol inlet. Alternatively, from 10 to 22 min and 45 to 56 min the gas stream was routed through the particle filter line we employ. For the first trial, the average measured extinction coefficients and 95% confidence intervals were 42 ± 3 and 43 ± 3 Mm^{-1} for with and without the particle filter, respectively. For the second trial, the mean extinction coefficients were 44 ± 2 and 44 ± 1 Mm^{-1} for before and during filtering, respectively. No significant loss of NO_2 was noted when the airstream was passed through the filter under our operational conditions. Two trials of a similar experiment for ozone are presented in Figure 4B. In this experiment, ozone was generated in air by irradiation with a UV mercury pen lamp. The lamp was turned on at t = 10 min and the ozone concentration in the airstream passing through the aerosol inlet allowed to reach a constant value of 8300 ± 300 ppbv (mean ± 95% C.I.). At t = 22 min, the airstream was routed through the particle filter. Immediately, a drop in ozone concentration and associated extinction was observed. For this trial, the ozone concentration dropped to 7700 ± 80 ppbv when being pulled through the particle filter. Similar results were observed for a second experimental trial (aerosol inlet = 8800 ± 200 ppbv, filtered air = 8100 ± 100 ppbv). In general, both optical data and the ozone monitor reflect a loss of ≈8% of the ozone by virtue of passage through the HEPA filter. This result suggests this effect could pose a potential error in experiments in which ozone concentration is very high (such as chamber studies). However, for ambient monitoring applications this loss of ozone would not be measurable. To explain, first consider the potential for ozone interference within the confines of an ambient aerosol monitoring experiment. If O_3 concentration is roughly 40

ppbv (typical of troposphere), even if particle filtering was to remove all ozone from the sample, the change to extinction would be <<1 Mm^{-1}, a value very near the instrument limit of detection. A loss of 8% in this concentration regime would not be detectable. Indeed, measurement uncertainty much larger than this is induced through statistical fluctuations of the number of particles within the probe beam volume. Therefore, for ambient monitoring applications, changes in ozone concentration induced by performing zero air measurements by the HEPA filters we employ should not cause significant error for measurement of aerosol extinction.

An alternate source of potential error would be changes in ambient levels of NO_2 between instrument calibration and ambient aerosol measurements. This could lead to either an underestimation or over estimation of aerosol b_{ext} depending on the direction of change. In an effort to assess the magnitude of this potential problem at our location, we have studied the variance of replicate data points for extinction measurements on filtered air samples from the ambient atmosphere. Filtering the air removes particles, so only changes in gas-phase absorption should be sensed on the extinction channel. We have broken data collected into 30 min long time bins, since this would be an easily achieved and convenient instrument calibration frequency. Since the main light absorbing gas of interest (NO_2) is photochemically active, we have also conducted measurements after sunset in an attempt to uncover differences between night/day measurements. In addition, we have studied the variance of measurements for an experiment in which the measurement cell is filled with filtered air and then sealed. This value represents a limit of performance of the instrument itself excluding effects of absorbing gases.

The mean observed variance for filtered air samples during daylight hours was 0.89 $(Mm^{-1})^2$ for N = 32 30-min wide time bins. The mean observed variance for filtered air samples during evening hours was 0.94 $(Mm^{-1})^2$ for N = 23 bins. The average variance when the optical cell was filled with filtered air and then sealed was 0.47 $(Mm^{-1})^2$ for N = 14 bins. These results illustrate the variance in optical data is larger than the instrumental limit when making filtered air measurements in both night and day. This suggests that variation in absorbing gas concentrations may affect aerosol extinction measurements, although the effect appears to be fairly small for most cases.

The variance for nighttime measurements was slightly larger than for the day. This may be a consequence of beginning experiments soon after sunset. These measurements have been made in January to early February when sunset at our location occurs between 5:30 and 6:30 p.m. Many vehicles are still on the road at this time, and on at least one occasion a substantial increase in filtered air extinction coefficient was noted in the early evening hours immediately after sunset. The combination of significant fuel combustion and lower actinic flux (decreased photolysis rate) may allow concentration of NO_2 to build rapidly. It should be noted that an opposite trend in b_{ext} was noted on at least one occasion after sunrise. Therefore, for our location the transition periods between day/night seem to be particularly susceptible to systematic error in aerosol b_{ext} measurements resulting from incomplete/improper subtraction of absorbing gas extinction.

If measurements on-board aircraft or at locations where NO_2 is known to change rapidly are required, it is recommended that simultaneous NO_2 measurements be

performed with an instrument of superior temporal resolution. Optical extinction from NO_2 can then be computed from the known absorption cross section and used to correct the aerosol extinction data. Alternatively, a second CRDS optical cell could be included in the design that makes simultaneous extinction measurements on filtered air. This reference channel could be used to directly correct measurements. Finally, if the application would allow, more frequent blank measurements could be taken. Nonetheless, empirical results suggest the filtered air blank method is effective for extinction measurements on ambient aerosols provided regular filtered air blank measurements are carried out and the concentration of NO_2 does not change rapidly.

2.3.4 Effect of Number of Particles within the Probe Beam on Precision

Precision measured when filtered air fills the measurement chamber generally affords detection limits <1 Mm^{-1} on both the scatter and extinction channel. However, when particles are placed in the measurement chamber, the observed precision can become significantly worse. Pettersson *et al*.[18] have considered uncertainty in CRDS extinction measurements caused by statistical fluctuations in particle counts within the probe laser beam volume. These authors report relative uncertainty ($\Delta b_{ext\ stat}/b_{ext}$) for a collection of monodisperse particles can be given by

$$\left(\frac{\Delta b_{ext\,stat}}{b_{ext}}\right) = \frac{1}{\sqrt{NVRt}} \tag{5}$$

where N is particle number density, V is the probed volume, R is repetition rate of the laser, and t is the sampling time. We would then expect an inverse square root dependence of relative uncertainty with aerosol concentration, and consequently aerosol

extinction and scattering coefficient. Since the probe laser beam volumes in CRDS experiments are << 1 cm^3, statistical fluctuations can potentially be a major source of uncertainty.

In an effort to better understand this effect, we have examined how relative uncertainty scales with extinction and scattering for size-selected 440 nm diameter ammonium sulfate particles. In these experiments, aerosol was loaded into the optical cell and the cell was sealed. We elected to perform the experiment this way to get a true indicator of measurement precision rather than detect drift in aerosol source generation rates. No mirror purge flow was used which proved acceptable for short periods of time. Figure 5 illustrates plots of observed relative standard deviation for scattering and extinction coefficient measurements (s_{scat}/b_{scat} and s_{ext}/b_{ext}) plotted against particle number concentration. The solid line represents $1/\sqrt{N}$ scaling. As observed, when particle number density was low, the relative standard deviation (RSD) of both measurements could exceed 0.2. At higher number densities, the $1/\sqrt{N}$ scaling factor was a reasonably good fit to data and both RSDs approached a value of ≈0.05. This was not simply a consequence of higher values of extinction and scatter since the RSD for R-134a calibration gas of similar extinction (b_{scat}, $b_{ext} \approx 70$ Mm^{-1}) was 0.01-0.03, less than that typically observed for aerosol samples.

Laser theory allows computation of beam diameter for a symmetric, stable resonator such as we employ here.[51] Applying the equation for beam diameter for a stable Gaussian resonator from ref 51 while assuming a cylindrical beam (in reality, beam waist at center of resonator slightly smaller spot size) suggests a volume of roughly 0.069 cm^3

for the probe beam. At the lowest N, we have considered here, on average only 1-2 particles would occupy the probe beam at any given instant. Despite the data not being a perfect fit to the model at low N, the drastic increase in relative standard deviation for scattering and extinction in this concentration region suggests fluctuations in particle count within the probe beam may limit precision for measurement of b_{scat} and b_{ext}. It should also be noted that the particle position and orientation within the beam is of consequence for CRDS extinction measurements.[52, 53] Furthermore, the truncation angle for the sphere nephelometer we employ would be expected to differ for particles positioned at different points along the beam axis.[48]

Figure 5 also presents the measured relative standard deviations of albedo (s_ω/ω) as a function of particle number density for sealed cell experiments. The second x-axis of the figure provides approximate extinction coefficients for reference. The data points represent the standard deviations for 1 min averages. The gray line in the figure is the relative precision in albedo expected from the propagation of precision observed in scatter and extinction coefficient (s_{scat}/b_{scat} and s_{ext}/b_{ext}). The gray line assumes the b_{scat} and b_{ext} measurements are not correlated. As the figure illustrates, the observed RSDs in albedo were considerably less than that suggested by simply propagating uncertainty. This is likely due to the nature of albedo being an intrinsic property that is not dependent on the number of particles within the beam (i.e., particle count effects canceling out for scattering and extinction). The precision of the albedo measurement does degrade at low N when there are <10 particles in the beam on average. This could be a consequence of differences in truncation angle/error for individual particles in the beam at differing

locations within the sphere. This phenomenon is a significant limitation of the technique we describe at low N and future efforts should focus on examining, reducing, or eliminating this effect. However, this general measurement limitation (e.g., variability of particle count/type/orientation in measurement volume at low N) extends to other measurement techniques as well. For instance, Lack *et al*.[43] have used a multipass Herriot cell in a photoacoustic spectrometer to increase sample volume for aerosol absorption measurements. These authors have reported precision of no worse than 6% for the photoacoustic setup. Nonetheless, an important advantage of simultaneous measurement of scattering and extinction on the same set of particles is the potential for improving the precision of the albedo measurement. Figure 5 illustrates we have achieved such an improvement when compared to that expected for uncorrelated measurements. If albedo is computed by combining measurements with two different instruments, even if the aerosol sample is routed through the instruments sequentially without particle losses, it is virtually assured that both measurements will not take place on the exact same particles in the exact same orientation. This is particularly important when taking measurements at low number densities, when using techniques with very small probe volumes, and/or when comparing optical measurements taken by instruments with vastly different probed volumes (for example, CRDS and conventional nephelometry). If further efforts better constrain the location of particles within the sphere nephelometer and sensitivity can be enhanced, the potential for making single particle albedo measurements may exist.

In an effort to compare the precision we report with other methods, we consider a recent paper by Massoli *et al*.[33] These authors report uncertainty in albedo when

considering measurements by combinations of CRDS, nephelometry, and photoacoustic spectroscopy. The authors have suggested that combining nephelometry (TSI nephelometer) and CRDS results in an uncertainty in albedo of roughly 3-5% when $\omega > 0.8$, as is typically encountered in the ambient atmosphere. In comparison, they report an uncertainty of <2% for this same range when photoacoustic absorption measurements are combined with CRDS extinction measurements. We report (in Figure 5) a relative measurement precision of roughly 2.7% for sequential measurements when N = 220 cm^3. To a rough (and unfortunately painfully unsophisticated) approximation this appears to be superior to the combined CRDS/nephelometry approach reported by Massoli *et al*. but may not be as precise as the CRDS/photoacoustic combination. We also point out we are reporting a measurement precision while Massoli *et al*. report measurement uncertainty. Direct experimental comparisons between combined photoacoustic/nephelometry measurements and the device described herein should be carried out in the future to compare performance definitively.

2.3.5 Measurement Accuracy

In an effort to validate the accuracy of our optical measurements for aerosol samples we have made direct comparisons with the Mie theory of light scattering. This general approach has previously been used to validate CRDS measurements by a number of authors.[15, 18,19,22] The experiments involved generating aerosols composed of either ammonium sulfate (m = 1.52 + 0.00i) or nigrosin (absorbing dye, m = 1.72 + 0.28i), size selecting a particular diameter with an electrostatic classifier, performing optical measurements, and measuring the particle number concentration at the cell outlet. Plots

of extinction and scattering coefficient (cm^{-1}) versus particle number concentration (no. of particles/cm^3) are then prepared. A best fit line was applied to the data, and the slope of this line represents the observed optical cross sections. Figure 6 illustrates an example of such plots for size selected 330 nm diameter (A) ammonium sulfate and (B) nigrosin.

As observed, plots for extinction and scattering nearly overlap for ammonium sulfate ($\omega_{theo} = 1$) but as expected diverge substantially for the absorbing nigrosin dye ($\omega_{theo} \approx 0.54$). We have conducted this analysis for ammonium sulfate and nigrosin particles with diameters of 450, 630, and 780 nm. Quantitative results from experiments and theoretical values are presented in Figure 7. Theoretical values for extinction, scattering, and absorption efficiencies (Q terms) were retrieved from a freely available Mie code (MiePlot) and used to compute optical cross sections based on the known diameter. The results presented in Figure 7 demonstrate relatively good agreement between experiment and theory. Measured optical cross sections (gray bars) were within a standard deviation of the theoretical values (unshaded bars) in 13/16 experimental trials. As particle size increased, the standard deviation of the slopes tended to increase and the data points in each plot such as that shown in Figure 6 became more scattered. This is likely a consequence of low number count of particles within the probe beam (vide supra). The largest departure from theoretical values occurred for the scattering cross section for 980 nm diameter nigrosin particles. For extinction cross sections, only the 450 nm nigrosin particles yielded data for which the theoretical value lies outside the range defined by the mean ±1 s. It should be noted the standard deviation for this measurement series was unusually small (0.01×10^{-8} cm^2). The reasonably good match between measured optical

cross sections and theoretical values suggest accurate measurements are possible through the graphical approach described.

The experiment illustrated in Figure 4B also provides an additional accuracy check for the CRDS experiment. At the conditions of temperature and pressure for this experiment, ozone exhibits a weak visible absorption of 0.006 05 Mm^{-1}/ppb at 532 nm. Converting the CRDS extinction data to average concentration yields 8400 ± 200 and 7600 ± 200 ppbv for the two sample lines for trial 1 of the experiment. As previously mentioned, the ozone concentrations reported by the independent ozone monitor (2B Technologies) was 8300 ± 300 and 7700 ± 80 ppbv for trial 1. For trial 2, the CRDS data would yield 8600 ± 200 and 7800 ± 80 ppbv for before/after valve switching. The reference method yielded 8800 ± 200 and 8100 ± 100 ppbv (all data reported here is the mean ± 95% C.I.). The CRDS extinction data yields ozone concentrations essentially identical to those reported by the independent measurement. This provides additional evidence for confidence in the accuracy of the CRDS extinction measurements developed.

2.3.6 Effect of Transparent Tube on Optical Measurements

A very important finding regarding the inclusion of the transparent tube is summarized in Figure 8. The average albedo value that was computed when considering individual, simultaneous measurements of b_{scat} and b_{ext} (as opposed to the slopes of the lines) for ammonium sulfate aerosol tended to be lower than 1 for many particle sizes considered. The observed albedo decreased as particle diameter increased. Clearly this effect represents a measurement error since $\omega = 1$ for ammonium sulfate. We believe this

is likely a consequence of forward scattered light not being effectively sampled by the integrating sphere. There are two potential mechanisms for this. First, light scattered into the regions at the ends of the tube may not be effectively redirected back into the sphere for detection. The coated region at each end is a cylinder of approximately 7.6 cm in length and an internal diameter of 3.8 cm. Each end features a 1.25 cm diameter sample port to introduce/remove aerosol from the cell and 0.635 cm diameter holes to allow propagation of the laser beam. The holes themselves are not coated with Duraflect and it would be logical to assume all light incident on these regions is removed and not collected. An additional, and potentially more significant, loss mechanism is the reflectance material is only ≈95% reflective. By assuming random direction of light propagation in the coated cylinder (after scattering off wall), we describe the probability of light returning to the glass tube simply by envisioning an imaginary disk placed at the end of the glass tube and computing the ratio of the surface area of this imaginary disk to the total surface area of the coated cylinder. This treatment suggests the surface area through which photons can return to the tube (imaginary disk) is about 10% of the total area of the coated cylinder. This may suggest light scattered into the coated cylinder may undergo approximately 10 reflections prior to returning to the glass tube. Propagation of the 0.95 reflectivity through 10 reflections yields an effective reflectivity of only ≈0.6. Therefore, light scattered into the end of the tubes is likely not redirected into the sphere with high efficiency. This biases light collection efficiency as a function of scattering angle.

A second, related mechanism to explain this result is reflection of scattered light off the walls of the glass tube. Fractional reflectance of incident radiation striking a surface can be described by the Fresnel equation. A consequence of this equation is reflection is a function of incident angle, with it increasing dramatically above 60° incident angle. Furthermore, reflection will vary with polarization state. The integrating sphere nephelometer design aims to collect scattered light with equal efficiency over all scattering angles. This would minimize measurement biases associated with nephelometer calibration. However, when a glass tube is used to contain the scattering sample, differential reflection with incident angle at the air-glass interface can bias scattered light collection efficiency and degrade performance. For future devices, it is recommended that empirically based correction factors such as those provided by Figure 8 be determined to account for this bias. Correction factors to account for similar effects in conventional aerosol nephelometry have previously been reported and are commonly employed.[35,36] It is envisioned that an alternate approach to solve this problem could be calibrating the scattering channel with aerosol samples of $\omega = 1$. In this condition, $b_{scat} = b_{ext}$ and the CRDS measurement (which is based on first principles not calibration) could be used to provide an extinction measurement with which to calibrate the scattering channel. However, since underestimation of scatter coefficient appears to be a function of particle size, the size distribution and composition of the calibration particles should closely mimic those on which subsequent measurements will be taken. Because of the complexities associated with achieving this match, this proposed procedure was not attempted in this work.

2.3.7 Ambient Measurements on Dust-Dominated Aerosol

The afternoon of January 22, 2010 was unusually warm in Lubbock, TX (75 °F). The low ambient relative humidity (≈ 20%) and strong winds from the WSW at 35-42 miles/h created conditions conducive to soil dust being entrained into the atmosphere. During this period of time, we sampled ambient air through a laboratory window into an ≈20 ft long section of 3/8 in. diameter stainless steel tube at 8.3 L/min. The sample collected was routed into the optical cell for measurement. Figure 9 illustrates the observed values for b_{scat} and b_{ext} from approximately 2 to 5 p.m. local time on 1/22/2010 at our location. An additional data series presenting $PM_{2.5}$ mass concentration data (microgram per cubic meter) collected with a TEOM instrument at a site approximately 1.8 km to the east is also shown in the figure. As observed, the scattering and extinction coefficients ranged between 50 and 120 Mm^{-1} during this time (the event was a relatively mild dust storm). In our experience, it is very common that aerosol b_{scat} and b_{ext} at our location is <20 Mm^{-1} on days when dust is not blowing so this data set represents a significant departure from the norm. A good correlation is observed between the $PM_{2.5}$ and optical data. The $PM_{2.5}$ data seems to lag the optical data by approximately 1 data point. This could be a consequence of the travel time of dust from our location to the other sampling site given they are not colocated. The observed albedo is plotted on the second y-axis of Figure 9. As observed, single scatter albedo values ranged from 0.8 to 0.9 for the dust dominated aerosol. Average albedo of the dust dominated aerosol at 532 nm for this data set was 0.858 with a 95% confidence interval of ±0.005. This albedo is lower than values recently reported for other wind-blown dusts at similar wavelength.[47] However, substantial uncertainty exists in the direct comparison since absorption by dust

is influenced strongly by hematite content and mixing state. For instance, Linke *et al*. have reported a SSA of 0.98-0.99 for a resuspended Saharan dust sample collected in Cairo and Morocco.[54] Schladitz *et al*. have reported an albedo of 0.96 at 537 nm for Saharan dust sampled at Tinfou, Morocco.[55] Alternatively, Pandithurai *et al*. have used a radiometer to describe optical properties of dusts in New Delhi that are believed to have originated in the Thar desert.[56] These authors reported an average SSA value of only 0.79 for 500 nm wavelength. However, absorption by hematite strongly increases with shorter λ, so direct comparison with our measurements is difficult. Further complexity is encountered since Sokolik and Toon have reported that aggregation of hematite with other minerals can result in enhanced absorption. These authors project SSA values between 0.8 and 0.9 can be observed for a 1% hematite volume mixing ratio in certain aggregates.[57] Claquin *et al*. report the hematite content of soils in the silt fraction near our location is 1-2% m/m.[58] These authors also use a two-layer Mie code using a model for dust particles in which hematite coats quartz, clays, calcite, and feldspar. This model system allows prediction of a midvisible (550 nm) SSA value of 0.92-0.94 for dust aerosols typical of our location.[58] Extrapolating to our measurement wavelength (532 nm) would be expected to result in a lower albedo due to stronger absorption. While the measured albedo in this report is at the low end of the range currently believed to be representative of mineral dusts, uncertainties in iron content, mixing state, postentrainment modification, and contamination by local sources (campus buses. etc.) allow the measurement reported to be within a range of values that could be rationalized. While attempts have been made to chemically characterize dust at our location,[59]

additional work in this field is needed to begin modeling dust optical properties for West Texas.

2.4 Conclusions

A second generation device for simultaneous measurement of aerosol optical extinction and scattering is presented. Confining the aerosol sample to a transparent tube allows substantial reduction in sample volume and a corresponding improvement in temporal response when compared with the previous device. Use of the tube also constrains the optical path better than the previous device. However, reflections at the tube surface can lead to underestimation of aerosol scattering coefficient if calibration is performed with gases. Use of electrically actuated valves under computer control allow for automated calibration procedures to be developed, which could be employed for long-term unattended monitoring applications. The effect of filtering particles on ozone and NO_2 concentration in the gas stream has been studied. Loss of NO_2 was not noted, and while some loss of ozone in the filter line was observed, we suggest this would not be relevant to aerosol measurements under typical atmospheric concentrations of ozone. Optical extinction and scattering measurements have been performed on size-selected absorbing and nonabsorbing laboratory generated aerosols. Scattering and extinction cross sections have been measured and compared to the Mie theory of light scattering. Measurement precision for the scattering and extinction channels both seem to be limited by statistical fluctuations in the number of particles within the beam at low number concentrations. Given the small probe beam volumes typical of CRDS experiments (we project $\approx$0.069 cm^3 here) it is not uncommon to have <10 particles in the beam at any

instant when reproducing atmospheric levels of extinction with size-selected aerosols. It is envisioned that this effect could be of substantial significance for albedo estimates in which optical data from two independent instruments is combined. This could be particularly problematic when the measurement devices feature vastly different probed volumes. Designing CRDS optical resonators with larger beam volume (for instance by decreasing mirror radius of curvature toward a more confocal resonator) would be an encouraged design feature since relative precision caused by this effect is expected to scale with the inverse square root of number of particles in the beam. Nonetheless, the simultaneous measurement of b_{scat} and b_{ext} on the same sample volume results in an observed measurement precision in their ratio (albedo) that is considerably lower than that expected through simply propagation of uncertainty in the scattering and extinction measurements. This result is not surprising, considering the measurements we describe are simultaneously carried out on the same sample.

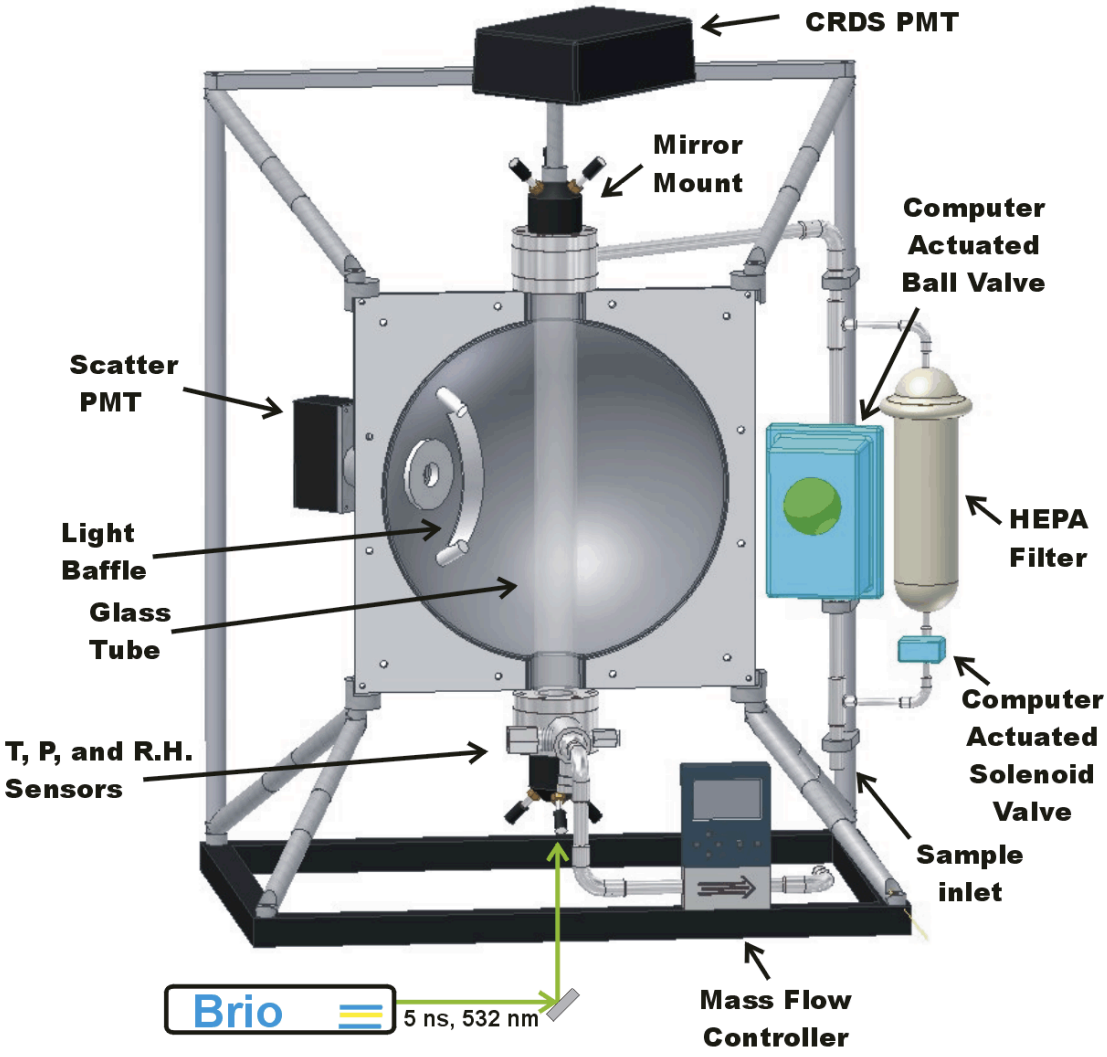

Figure 2.1. Illustration of the instrument for simultaneous measurement of scattering and extinction.

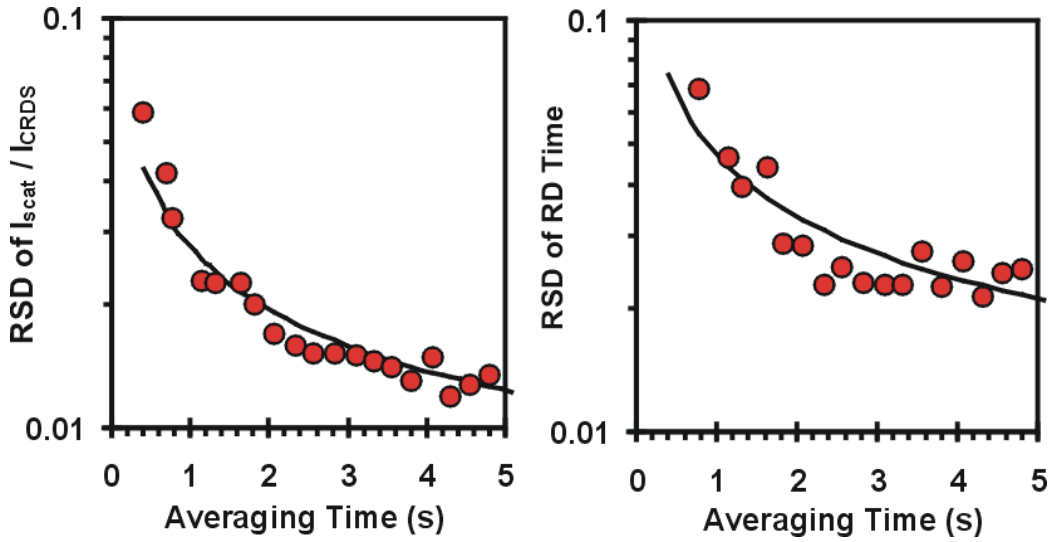

Figure 2.2. The effect of signal averaging time on relative standard deviation.
The effect of signal averaging time on relative standard deviation of (A) I_{scat}/ICRDS and (B) ring-down time when filtered air filled the optical cell. The solid lines represent a $1/\sqrt{t}$ scaling.

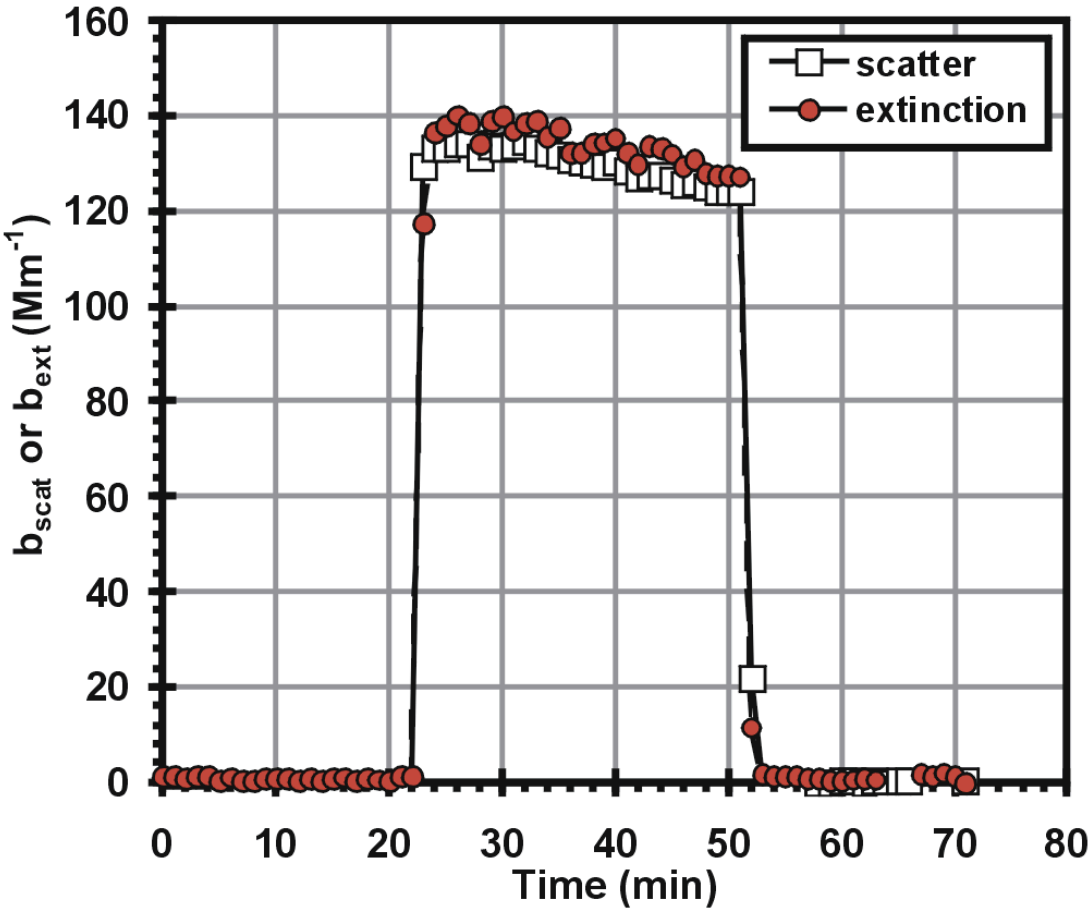

Figure 2.3. Instrument response for scattering and extinction coefficient on a polydisperse aerosol sample.
Instrument response for scattering (□) and extinction (red circles) coefficient following introduction of a polydisperse, submicrometer $(NH_4)_2SO_4$ aerosol sample between t = 22 and 52 min. Experimental conditions: P = 0.89 atm, T = 299.6 K, R.H. = 15-23%.

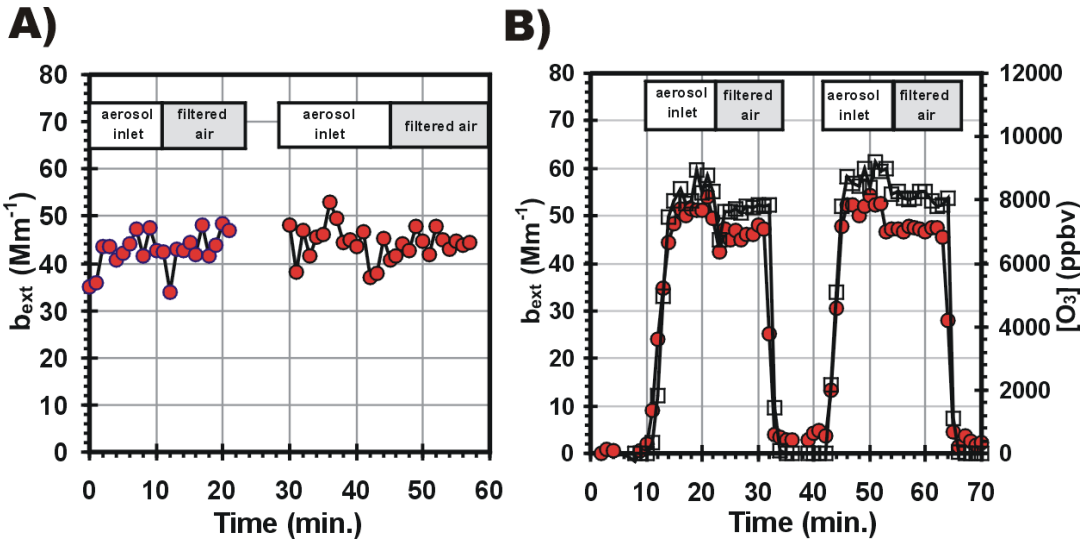

Figure 2.4. Effect of HEPA filter on the concentration of NO_2 and O_3.
Effect of HEPA filter on the concentration of (A) NO_2 and (B) O_3. In part B, ozone concentration (□) measured by a separate instrument is plotted on a second y-axis for clarity.

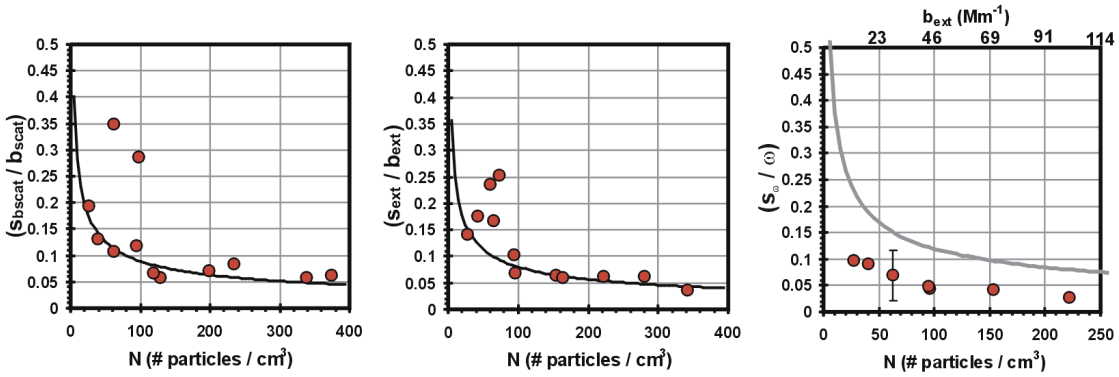

Figure 2.5. Observed relative precision in scatter coefficient, extinction coefficient, and albedo vs particle number density. Observed relative precision in scatter coefficient, extinction coefficient, and albedo vs particle number density (N) in the optical cell. The black solid lines represents 1/√N scaling and the gray line in the plot for albedo represents uncertainty expected from propagation of uncertainty in scattering and extinction. Particle number densities were computed through the optical data and Mie theory for ammonium sulfate Dp = 440 nm.

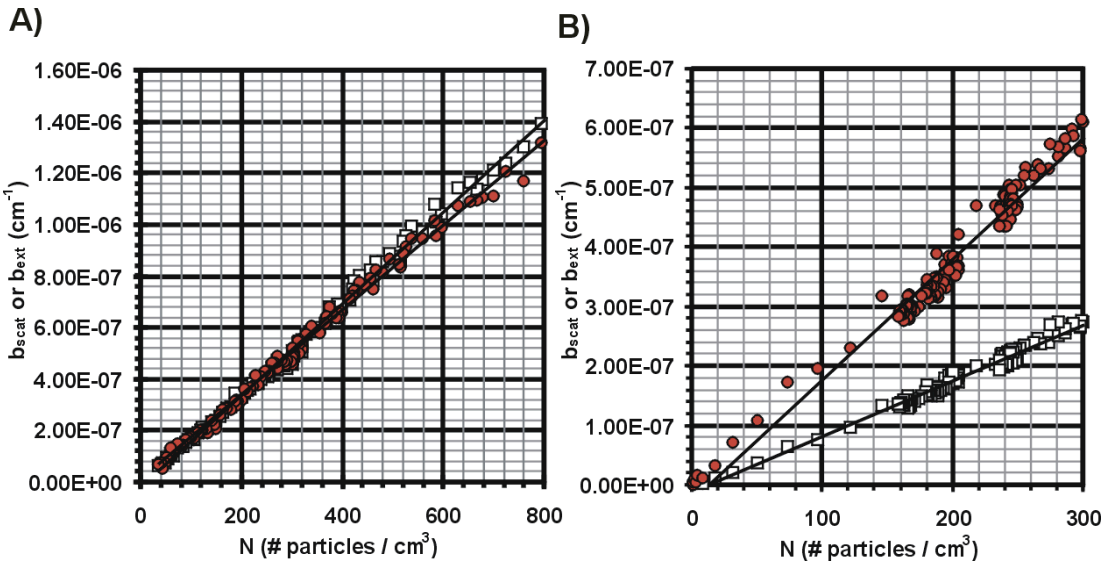

Figure 2.6. Plot of observed scattering and extinction coefficient vs particle concentration for $(NH_4)_2SO_4$ and nigrosin.

Plot of observed scattering (□) and extinction (red circles) coefficient vs particle concentration for size selected (Dp = 330 nm) (A) ammonium sulfate and (B) nigrosin. The slopes of the best-fit lines represent the scattering and extinction cross sections.

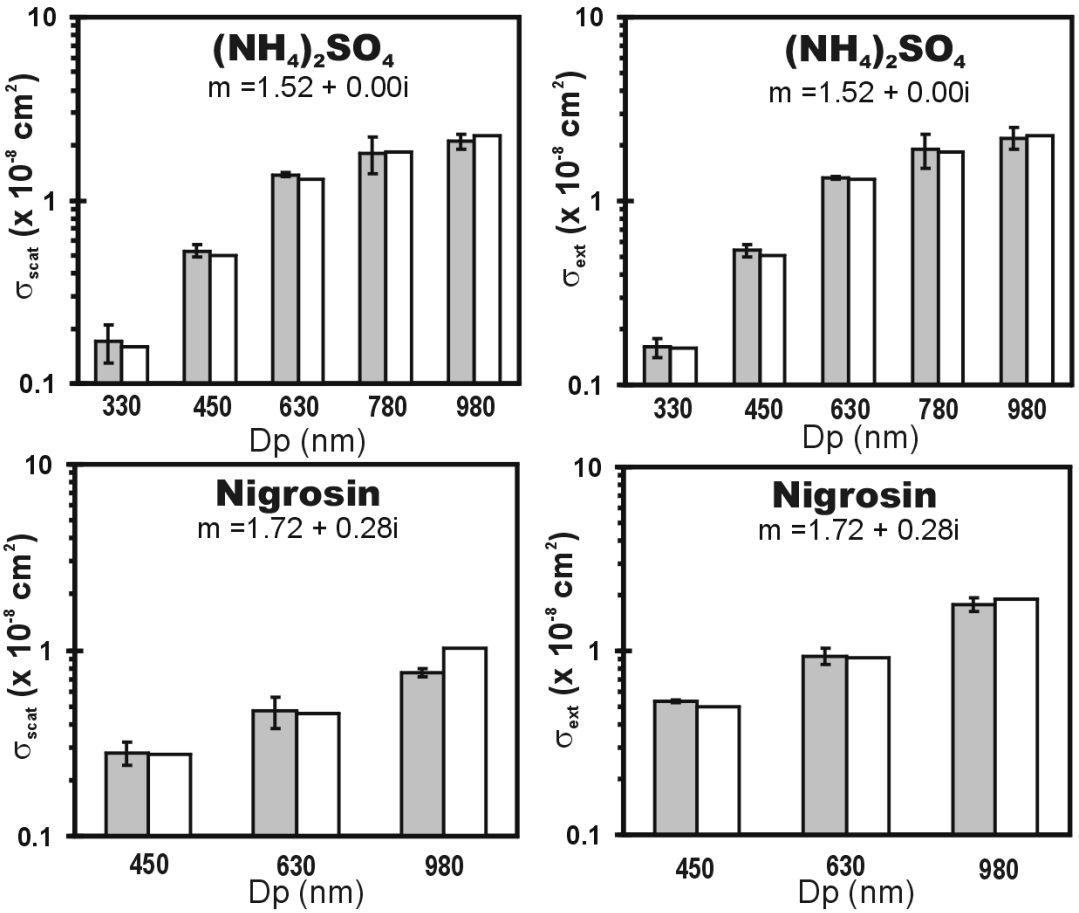

Figure 2.7. Comparison between measured and theoretical scattering and extinction cross sections (σ_{scat} and σ_{ext}) for $(NH_4)_2SO_4$ and nigrosin aerosol.
Gray bars represent measured values and white bars represent the theoretical values computed through Mie theory. Error bars are ±1 std deviation.

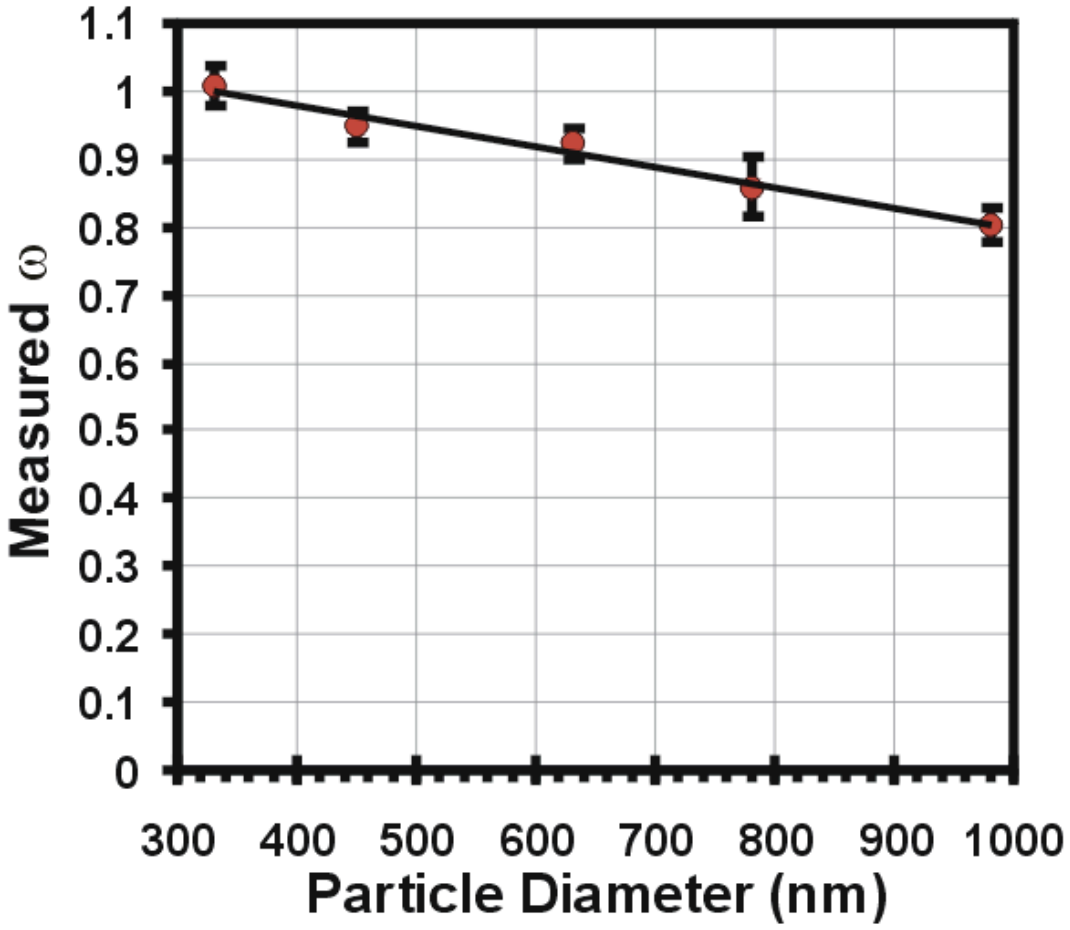

Figure 2.8. Observed average albedo from single point measurements vs particle diameter for $(NH_4)_2SO_4$ aerosol. Departure from unity suggests use of the transparent tube to contain the sample biases scattering measurements. Error bars are 1σ.

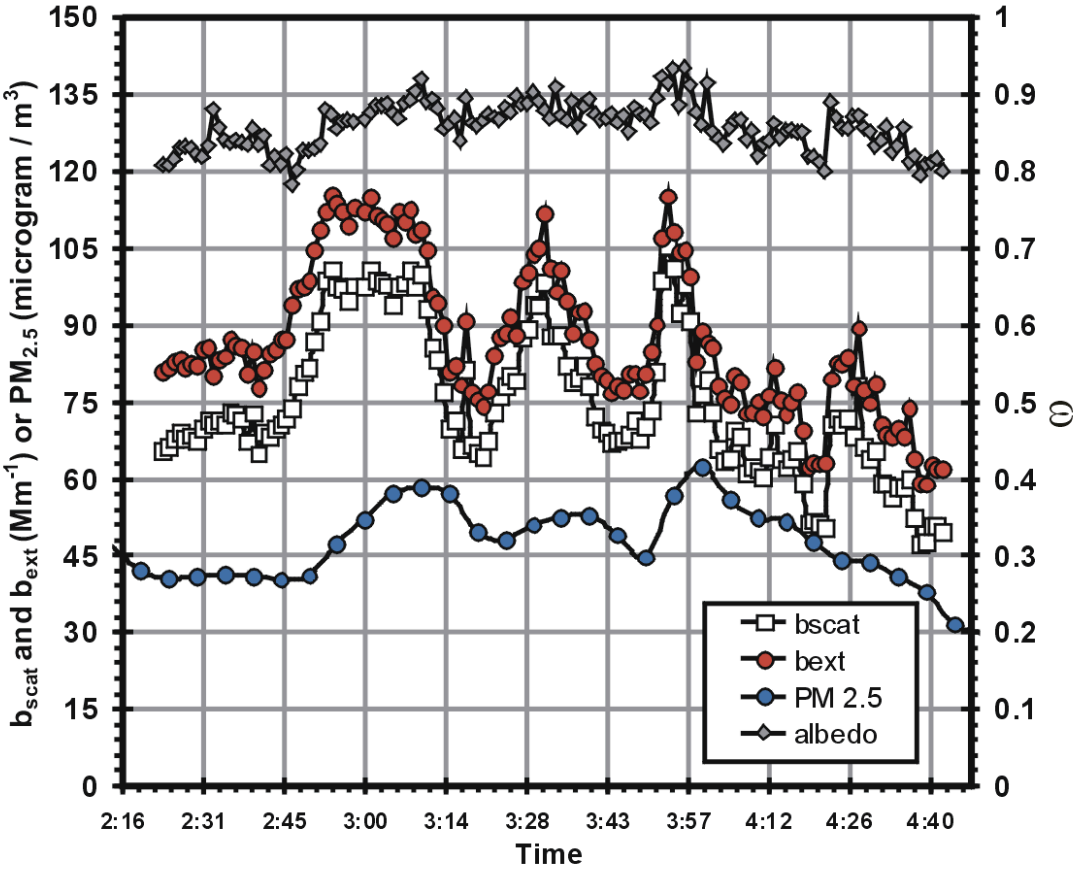

Figure 2.9. Ambient monitoring data from the afternoon of January 22, 2010 during a minor dust episode.
Optical data was collected in our laboratory. $PM_{2.5}$ mass concentration data was collected at a site approximately 1.8 km east of our location, which is a time delay of approximately 1.5 to 2 minutes.

2.6 References

[1] Ramaswamy, V. Radiative forcing of climate change. In *Climate Change 2001: The Scientific Basis. Contribution of Working Group I to the Third Assessment Report of the Intergovernmental Panel on Climate Change*; Houghton, J. T., Eds.; Cambridge University Press: Cambridge, U.K., 2001; pp 349-416.

[2] Huang,Y.;Dickinson,R.E.;Chameides,W.L.*Proc.Natl.Acad.Sci.U.S.A.* **2006**, *103* (12), 4371–4376.

[3] Lohmann, U.; Feichter, J. *Atmos. Chem. Phys.* **2005**, *5*, 715–737.

[4] Menon, S.; Hansen, J.; Nazarenko, L.; Luo, Y. *Science* **2002**, *297*, 2250– 2253.

[5] Charlson, R. J.; Schwartz, S. E.; Hales, J. M.; Cess, R. D.; Coakley, J. A.; Hansen, J. A.; Hofmann, D. J. *Science* **1992**, *255*, 423–430.

[6] Jacobson, M. Z. *Nature* **2001**, *409*, 695–697.

[7] Jacobson, M. Z. J. *Geophys. Res.* **2001**, *106*, 1551–1568.

[8] Dinar,E.;AboRiziq,A.;Spindler,C.;Erlick,C.;Kiss,G.;Rudich,Y.*Faraday Discuss.* **2008**, *137*, 279–295.

[9] Graber, E. R.; Rudich, Y. *Atmos. Chem. Phys.* **2006**, *6*, 729–753.

[10] Chang, J. L.; Thompson, J. E. *Atmos. Environ.* **2010**, *44*, 541–551.

[11] Shapiro, E. L.; Szprengiel, J.; Sareen, N.; Jen, C. N.; Giordano, M. R.; McNeill, V. F. *Atmos. Chem. Phys.* **2009**, *9*, 2289–2300.

[12] Smith, J. D.; Atkinson, D. B. *Analyst* **2001**, *126*, 1216.

[13] Thompson, J. E.; Smith, B. W.; Winefordner, J. D. *Anal. Chem.* **2002**, *74*, 1962–1967.

[14] Thompson, J. E.; Nasajpour, H.; Smith, B. W.; Winefordner, J. D. *Aerosol Sci. Technol.* **2003**, *37*, 221–230.

[15] Bulatov, V.; Fisher, M.; Schechter, I. *Anal. Chim. Acta* **2002**, *466*, 1–9.

[16] Moosmuller, H.; Varma, R.; Arnott, W. P. *Aerosol Sci. Technol.* **2005**, *39*, 30–39.

[17] Thompson, J. E.; Spangler, H. D. *Appl. Opt.* **2006**, *45* (11), 2465–2473.

[18] Pettersson, A.; Lovejoy, E. R.; Brock, C. A.; Brown, S. S.; Ravishankara, A. R. J. *Aerosol. Sci.* **2004**, *35*, 995–1011.

[19] Baynard, T.; Lovejoy, E. R.; Pettersson, A.; Brown, S. S.; Lack, D.; Osthoff, H.; Massoli, P.; Ciciora, S.; Dube, W. P.; Ravishankara, A. R. *Aerosol Sci. Technol.* **2007**, *41* (4), 447–462.

[20] Butler, T. J. A.; Mellon, D.; Kim, J.; Litman, J.; Orr-Ewing, A. J. *J. Phys. Chem. A* **2009**, *113* (16), 3963–3972.

[21] Strawa, A. W.; Castaneda, R.; Owano, T.; Baer, D. S.; Paldus, B. A. *J. Atmos. Oceanic Technol.* **2003**, *20*, 454–465.

[22] Lang-Yona, N.; Rudich, Y.; Segre, E.; Dinar, E.; Abo-Riziq, A. *Anal. Chem.* **2009**, *81* (5), 1762–1769.

[23] Abo Riziq, A.; Trainic, M.; Erlick, C.; Segre, E.; Rudich, Y. *Atmos. Chem. Phys.* **2008**, *8*, 1823–1833.

[24] Adler, G.; Abo Riziq, A.; Erlick, C.; Rudich, Y. *Proc. Natl. Acad. Sci. U.S.A.* **2010**, *107*, 6699–6704.

[25] Freedman, M. A.; Hasenkopf, C. A.; Beaver, M. R.; Tolbert, M. A. *J. Phys. Chem. A* **2009**, *113*, 13584–13592.

[26] Lang-Yona, N.; Abo-Riziq, A.; Erlick, C.; Segre, E.; Trainic, M.; Rudich, Y. *Phys. Chem. Chem. Phys.* **2010**, *12*, 21–31.

[27] Riziq, A. A.; Erlick, C.; Dinar, E.; Rudich, Y. *Atmos. Chem. Phys.* **2007**, *7*, 1523–1536.

[28] Spindler, C.; Riziq, A. A.; Rudich, Y. *Aerosol Sci. Technol.* **2007**, *41*, 1011–1017.

[29] Rudic, S.; Miles, R. E. H.; Orr-Ewing, A. J.; Reid, J. P. *Appl. Opt.* **2007**, *46*, 6142–6150.

[30] Heintzenberg, J.; Charlson, R. J. J. *Atmos. Oceanic Technol.* **1996**, *13* (5), 987–1000.

[31] Moosmuller, H.; Arnott, W. P. *Rev. Sci. Instrum.* **2003**, *74* (7), 3492–3501.

[32] Muller,T.;Nowak,A.;Wiedensohler,A.;Sheridan,P.;Laborde,M.;Covert, D. S.; Marinoni, A.; Imre, K.; Henzing, E.; Roger, J. C.; dos Santos, S. M.; Wilhelm, R.; Wang, Y. Q.; de Leeuw, G. *Aerosol Sci. Technol.* **2009**, *43* (6), 581–586.

[33] Massoli, P.; Murphy, D. M.; Lack, D. A.; Baynard, T.; Brock, C. A.; Lovejoy, E. R. *Aerosol Sci. Technol.* **2009**, *43* (11), 1064–1074.

[34] Ensor, D. S.; Waggoner, A. P. *Atmos. Environ.* **1970**, *4*, 481–487.

[35] Anderson, T. L.; Ogren, J. A. *Aerosol Sci. Technol.* **1998**, *29* (1), 57–69.

[36] Heintzenberg, J.; Wiedensohler, T. M.; Tuch, T. M.; Covert, D. S.; Sheridan, P. S.; Ogren, J. A.; Gras, J.; Nessler, R.; Kleefeld, C.; Kalivitis, N.; Aaltonen, V.; Wilhem, R. T.; Havlicek, M. J. *Atmos. Oceanic Technol.* **2006**, *23*, 902– 914.

[37] Varma, R.; Moosmuller, H.; Arnott, W. P. *Opt. Lett.* **2003**, *28*, 1007–1009.

[38] Fukagawa, S.; Kuze, H.; Lagrosas, N.; Takeuchi, N. *Appl. Opt.* **2005**, *44*, 3520–3526.

[39] Sedlacek, A. J.; Lee, J. *Aerosol Sci. Technol.* **2007**, *41* (12), 1089–1101.

[40] Sedlacek, A. J. *Rev. Sci. Instrum.* **2006**, *77*, 064903.

[41] Arnott, W. P.; Moosmuller, H.; Sheridan, P. J.; Ogren, J. A.; Raspet, R.; Slaton, W. V.; Hand, J. L.; Kreidenweis, S. M.; Collett, J. L. *J. Geophys. Res.* **2003**, *108*, (D1), 4034, DOI: 10.1029/2002JD002165.

[42] Lewis, K.; Arnott, W. P.; Moosmuller, H.; Wold, C. E. *J. Geophys. Res. Atmos.* **2008**, *113* (D16), D16203.

[43] Lack, D. A.; Lovejoy, E. R.; Baynard, T.; Pettersson, A.; Ravishankara, A. R. *Aerosol Sci. Technol.* **2006**, *40* (9), 697–708.

[44] Arnott, W. P.; Moosmuller, H.; Rogers, C. F.; Jin, T.; Bruch, R. *Atmos. Environ.* **1999**, *33*, 2845–2852.

[45] Arnott, W. P.; Hamasha, K.; Moosmuller, H.; Sheridan, P. J.; Ogren, J. *Aerosol Sci. Technol.* **2005**, *39*, 17–29.

[46] Moosmuller, H.; Chakrabarty, R. K.; Arnott, W. P. *J. Quant. Spectrosc. Radiat. Transfer* **2009**, *110*, 844–878.

[47] Redmond, H. E.; Dial, K. D.; Thompson, J. E. *Aeolian Res.* **2009**, DOI: 10.1016/j.aeolia.2009.09.002.

[48] Thompson, J. E.; Barta, N.; Policarpio, D.; DuVall, R. *Opt. Express* **2008**, *16* (3), 2191–2205.

[49] Schmid, O.; Artaxo, P.; Arnott, W. P.; Chand, D.; Gatti, L. V.; Frank, G. P.; Hoffer, A.; Schnaiter, M.; Andreae, M. O. *Atmos. Chem. Phys.* **2006**, *6*, 3443–3462.

[50] Bond, T. C.; Anderson, T. L.; Campbell, D. *Aerosol Sci. Technol.* **1999**, *30*, 582–600.

[51] Siegman, A. E. *Lasers*; University Science Books: Mill Valley, CA, 1986.

[52] Butler, T. J. A.; Miller, J. L.; Orr-Ewing, A. J. *J. Chem. Phys.* **2007**, *126*, 174302.

[53] Miller, J. L.; Orr-Ewing, A. J. *J. Chem. Phys.* **2007**, *126*, 174303.

[54] Linke, C.; Mohler, O.; Veres, A.; Mohacsi, A.; Bozoki, Z.; Szabo, G.; Schnaiter, M. *Atmos. Chem. Phys.* **2006**, *6*, 3315–3323.

[55] Schladitz, A.; Muller, N.; Kaaden, N.; Massling, A.; Kandler, K.; Ebert, M.; Weinbruch, S.; Deutscher, C.; Wiedensohler, A. *Tellus B* **2009**, *61* (1), 64–78.

[56] Pandithurai, G.; Dipu, S.; Dani, K. K.; Tiwari, S.; Bisht, D. S.; Devara, P. C. S.; Pinker, R. T. *J. Geophys. Res.* **2008**, *113* (D13209), DOI: 10.1029/ 2008JD009804.

[57] Sokolik, I. N.; Toon, O. B. *J. Geophys. Res.* **1999**, *104* (D8), 9423–9444.

[58] Claquin, T.; Schulz, M.; Balkanski, Y. J. *J. Geophys. Res.* **1999**, *104* (D18), 22,243–22,256.

[59] Gill, T. E.; Stout, J. E.; Peinado, P. *Applications of Accelerators in Research and Industry: 20th International Conference*, McDaniel, F. D., Doyle, B. L., Eds.; 2009, CP1099, pp 255-258.

Chapter III

Conclusion

3.1 Major Accomplishments and Findings

We have implemented and tested design improvements on the first generation albedometer. The addition of the glass tube in the second generation of the albedometer has drastically improved the temporal response of the instrument; the response is now less than a minute whereas the first generation instrument had a temporal response of 20 to 30 minutes. At the same time, the glass tube results in losses of some scattered light so that the calculated albedo tends to be smaller than it should be. While calculating a correction factor for this effect is possible, it is complicated due to the fact that this effect changes with particle size.

In general our instrument shows a good degree of precision. However, as the number of particles in the probe beam drops, the precision of our measurements is dopped as well. When the number density of the sample is high the RSD for both b_{ext} and b_{scat} is around 0.05, but these can increase to over 0.2 when the number density is low. We have shown that the measurements from the albedometer compare well to the calculations from Mie theory because for most trials, the σ_{ext} and σ_{scat} calculated from the measured b_{ext} and b_{scat} agreed with those calculated from Mie theory. This agreement is often within one standard deviation of the measurements. Finally, tests have shown that ozone as an absorbing gas will have minimal affect on measurements at ambient ozone levels. Testing with NO_2, however, have shown the need to be able to subtract out the contribution from this absorbing gas.

3.2 Future directions

Because the optical properties of aerosols are wavelength dependent, expanding the albedometer into other wavelengths will be a good avenue for exploration. Expanding the knowledge of how various aerosols interact with light in other regions of the spectrum (i. e., near-UV) will help to improve the accuracy of the climate change models. Since many atmospheric components are photochemically active in the UV and near UV regions, attenuation of this radiation is important.[1] Also, measuring absorption and scattering in this region is complicated because many atmospheric gases also absorb in this region.[2]

Minituarizing the instrument is also an area worthy of exploration. A smaller setup will increase portability. If possible, designing a casing to protect the unit from vibrations will allow mobile monitoring of ambient aerosols. However, miniaturizing the instrument will limit the sample volume further. Since atmospheric conditions generally have low concentrations of particles, the number of particles in the beam during measurement will be restricted beyond the current configuration. Since precision was found to suffer as particle concentrations drop, this will be a significant area of concern.

3.3 References

[1] Jaroslawski, J.; Krzyscin, J. W.; Puchalski, S.; Sobolewski, P. *J. Geophys. Res* **2003**, *108*, 1992.

[2] Corr, C. A.; Krotkov, N.; Madronich, S.; Slusser, J. R.; Holben, B.; Gao, W.; Flynn, J.; Lefer, B.; Kreidenweis, S. M. *Atmospheric Chemistry and Physics* **2009**, *9*, 5813.